Spatial molecular profiling of mixed invasive ductal-lobular breast cancers reveals heterogeneity in intrinsic molecular subtypes, oncogenic signatures and actionable driver mutations

Osama Shiraz Shah[1,3], Azadeh Nasrazadani[1,4], Julia Foldi[7], Jennifer M. Atkinson[1,2], Celina G Kleer[8], Priscilla F. McAuliffe[1,6,] Edaise M da Silva[9], Pier Selenica[9], Higinio Dopeso[9], Fresia Pareja[9], Diana Mandelker[9], Britta Weigelt[9], Jorge S. Reis-Filho[9], Rohit Bhargava[4], Peter C. Lucas[1,4,5], Adrian V. Lee*[1,2], Steffi Oesterreich*[1,2]

[1]Womens Cancer Research Center at UPMC Hillman Cancer Center and Magee Women's Research Institute, Pittsburgh, PA.

[2]Department of Pharmacology & Chemical Biology, University of Pittsburgh, Pittsburgh, PA.

[3]Integrative Systems Biology Program, University of Pittsburgh, Pittsburgh PA.

[4]Department of Pathology, University of Pittsburgh School of Medicine, Pittsburgh, PA

[5]NSABP Foundation, Inc., Pittsburgh, PA

[6]Division of Surgical Oncology, Department of Surgery, University of Pittsburgh School of Medicine, Pittsburgh, PA

[7]Division of Hematology-Oncology, Department of Medicine, University of Pittsburgh, Pittsburgh, PA.

[8]Department of Pathology and Rogel Cancer Center, University of Michigan Ann Arbor, MI 48109, USA

[9]Department of Pathology and Laboratory Medicine, Memorial Sloan Kettering Cancer Center (MSKCC), New York, NY, USA

Keywords: Mixed invasive ductal and lobular carcinoma, mDLC, digital spatial profiling, DSP, breast cancer, tumor heterogeneity, multi-omics, precision medicine

* Steffi Oesterreich and Adrian Lee share senior authorship

Corresponding Authors: Steffi Oesterreich, University of Pittsburgh, 5051 Centre Ave, Pittsburgh, PA 15213. Phone: 412-641-8555, Fax: 412-641-7724, E-mail: oesterreichs@upmc.edu. Adrian Lee, University of Pittsburgh, 5051 Centre Ave, Pittsburgh, PA 15213. E-mail: leeav@upmc.edu.

Graphical Abstract

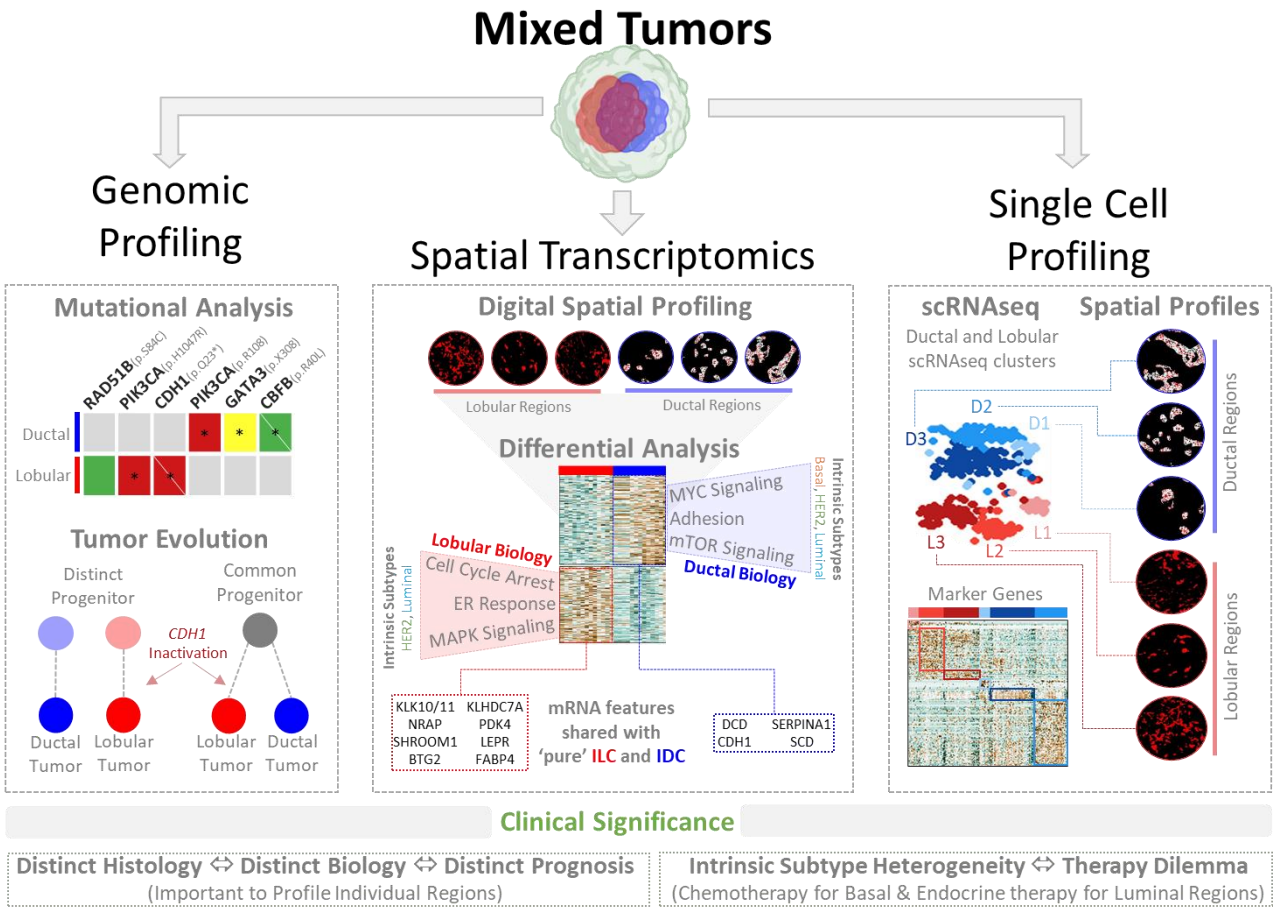

Abstract [N=135]

Mixed invasive ductal and lobular carcinoma (mDLC) is a rare histologic subtype of breast cancer displaying both E-cadherin positive ductal and E-cadherin negative lobular morphologies within the same tumor, posing challenges with regard to anticipated clinical management. It remains unclear whether these distinct morphologies also have distinct biology and risk of recurrence. Our spatially-resolved transcriptomic, genomic, and single-cell profiling revealed clinically significant differences between ductal and lobular tumor regions including distinct intrinsic subtype heterogeneity (e.g., mDLC with TNBC/basal ductal and ER+/luminal lobular regions), distinct enrichment of senescence/dormancy and oncogenic (ER and MYC) signatures, genetic and epigenetic *CDH1* inactivation in lobular, but not ductal regions, and 4) single-cell ductal and lobular sub-populations with unique oncogenic signatures further highlighting intra-regional heterogeneity. Altogether, we demonstrated that the intra-tumoral morphological/histological heterogeneity within mDLC is underpinned by intrinsic subtype and oncogenic heterogeneity which may result in prognostic uncertainty and therapeutic dilemma.

Significance [N=58]

mDLC displays both ductal and lobular tumor regions. Our multi-omic profiling approach revealed that these morphologically distinct tumor regions harbor distinct intrinsic subtypes and oncogenic features that may cause prognostic uncertainty and therapeutic dilemma. Thus histopathological/molecular profiling of individual tumor regions may guide clinical decision making and benefit patients with mDLC, particularly in the advanced setting where there is increased reliance on next generation sequencing.

Main Text

Introduction

Breast cancer is a prevalent disease worldwide[1] and is the most frequently diagnosed cancer in women in the US, with approximately 300,000 cases per year[2]. The majority (approximately 75%) of cases are classified histologically as invasive ductal carcinoma of no special type (IDC-NST). Invasive lobular carcinoma (ILC) is the most common special type accounting for approximately 10-15% of all invasive breast cancer diagnoses[3,4]. Apart from the well-defined histologic and tissue histological differences, there are numerous notable molecular distinctions between ILC and IDC-NST. ILC exhibits enrichment of *CDH1*, *FOXA1*, *TBX3*, *ERBB2* and *PTEN* alterations, while IDC-NST shows a higher frequency of *GATA3*, *MAP3K1*, *TP53* and *MYC* alterations[5]. As a result of *CDH1* alterations, ILC lacks E-cadherin expression, an important cell adhesion molecule[6], and display cytoplasmic p120 staining while IDC-NST retains membranous expression for both molecules[7]. Clinically, ILC is more common in elderly women, presents as larger tumors and is frequently multicentric and multifocal compared to IDC-NST[8,9]. ILC is usually detected later and leads to higher rates of mastectomy [10–14]. ILC is also associated with more frequent metastases to urogenital and gastrointestinal tracts as well as to serosal surfaces than IDC-NST[15,16]. Despite presenting with markers of favorable prognosis, such as low grade, low proliferation index, estrogen receptor positive and human epidermal growth factor receptor (HER2) low/negative, patients with ILC have a higher rate of late recurrences and worse long-term prognosis than those with IDC-NST[14,17,18]. Given its distinct prognosis and outcome compared to IDC-NST, ILC is increasingly being recognized as a distinct disease, yet it is still treated similarly to IDC-NST in the

clinic due to a lack of specific treatment guidelines[14,19,20]. Ongoing clinical trials focused on patients with ILC may lead to the development of more tailored and effective treatment options in the future[20].

Apart from ILC, there are numerous other special types of breast cancers such as mixed invasive breast carcinoma. This is an elusive group of breast cancers which the World Health Organization (WHO) defines as tumors presenting with areas of 10-90% of special histology (such as ILC) admixed with at least 10% of IDC-NST[21]. Mixed tumors comprising of both ILC and IDC-NST are the most common (~5-10% of all breast cancer cases[22–27]) and are termed mixed invasive ductal and lobular breast carcinoma (mDLC)[28]. Despite increasing incidence of mDLC[29,30], it remains understudied, leading to diagnostic and prognostic uncertainty and clinical management challenges for the patients with this elusive disease. Although there are limited reports focused on mDLC, a few seminal studies have provided insights into its complex pathobiology. Immunohistochemical (IHC) studies have confirmed while that ductal regions of mDLC retain membranous E-cadherin, while lobular regions either lose or display aberrant E-cadherin IHC staining[31–33]. Clinical studies have often yielded contradictory findings[23–25,30,31,33–35], but overall, they suggest that mDLC is clinically more similar to pure ILC than IDC-NST[28,36]. These discrepancies may be due to the non-standardized and fluid definition of mDLC, limited consideration of its underlying tumor regions and their distinct features and proportions, and the vast intratumoral heterogeneity of this disease[28,30,37,38]. Misdiagnosis is also possible, particularly if only one of the two histologic regions is identified in the diagnostic biopsies[28,30,37,38]. Notably, accurate diagnosis of mDLC remains a challenge[28,30,37,38] and traditional diagnostic methods, such

as mammography, may prove inadequate, as they are often less sensitive in detecting lobular tumors owing to their diffuse growth pattern[13,14,39–41]. However, the use of magnetic resonance imaging (MRI) and E-cadherin IHC assessment in biopsy specimens can improve diagnostic accuracy[20,42,43]. Moreover, molecular studies with profiling of individual tumor regions have been limited and largely focused on analysis of somatic genetic alterations. While these have provided valuable insights into the tumorigenesis pathways and distinct mutational landscape of ductal and lobular tumor regions[33,44], comprehensive studies delineating transcriptomic differences between these distinct regions have not been performed.

To fill this knowledge gap, we employed spatially resolved transcriptomic, genomic, and single cell profiling approaches to comprehensively investigate mDLC and highlight its intratumoral heterogeneity and complexity. We delineate the biological and intrinsic subtype differences between its underlying ductal and lobular tumor regions. Notably, our findings highlight that in some mDLC cases distinct tumor regions with distinct biology may pose distinct progression risk. Hence histopathological and molecular profiling mDLC and its individual tumor regions may inform treatment decisions.

Results

Patient Specimens and Their Clinicopathologic Characteristics

A panel of three molecular pathologists identified invasive breast cancer cases diagnosed as "mixed invasive ductal and lobular carcinoma" and shortlisted three cases for this pilot study. All three cases were reported as estrogen receptor positive (ER+) and HER2 negative/low and their ages ranged from 46-63 years (Fig. 1A, Supplementary Table S1A). Assessment of H&E and E-cadherin/p120 dual staining confirmed that each case exhibited histomorphic features in line with the latest mDLC definition i.e., admix of E-cadherin negative lobular tumor regions with at least 10-90% of E-cadherin positive ductal tumor regions (Supplementary Table S1B). Importantly, overall, these cases exhibited collision of spatially distinct ductal and lobular tumor regions[68,78] along with some regions of intermixing and hence could be broadly defined as mDLC of "collision" type. These cases were particularly amenable for downstream multi-omic profiling compared to those that exhibited more intermingling or intermixing with close proximity of histologic tumor regions. Clinical diagnostic and treatment timelines of these cases, source of their tumor tissue used in this study, and their histomorphic features are illustrated in Fig. 1A. Both MDLC-2 and MDLC-3 eventually developed recurrent disease resulting in patient death in the case of MDLC-2. As of the last follow-up in 2022, both MDLC-3 and MDLC-1 are alive, and MDLC-1 remains free of recurrent disease.

Whole-Transcriptome Spatial Profiling of Ductal and Lobular Regions

To better understand the biological heterogeneity and transcriptomic features of ductal and lobular regions, we performed whole-transcriptome digital spatial profiling (DSP) of these three

133 mDLC cases. In total, we analyzed 26 regions of interest (ROIs) with at least 6 ROIs per case.
134 Selected ROIs from a representative case (MDLC-3) are shown in Fig. 1B. We segmented ductal
135 and lobular areas using E-cadherin and Pan-CK staining (Fig. 1C). This enabled profiling of pure
136 ductal and lobular areas from heterogeneous regions that were predominantly of one histology
137 or a mixture of both (Fig. 1D). E-cadherin expression in segmented ductal and lobular regions
138 showed expected results (Fig. 1E). All profiled regions had high RNA sequencing saturation (>
139 94%) and low noise (Q3 count > Negative probe count). However, three regions had low read
140 count (< 0.3 million) and were excluded from further analysis (Supplementary Fig. S1A-C). Our
141 final DSP dataset is comprised of 13 ductal and 13 lobular regions.

142 **Transcriptomic Clusters and Intrinsic Molecular Subtypes**

143 Exploration using top variable genes revealed that regions from each tumor clustered based upon
144 their histology (Fig. 2A; Supplementary Fig. S1D). MDLC-3 ductal regions showed the most distinct
145 mRNA expression compared to all other regions. PAM50 analysis showed both inter and intra-
146 tumor heterogeneity of prognostically relevant intrinsic molecular subtypes (IMS). MDLC-2 ductal
147 regions were a mix of Luminal A and HER2-Enriched subtypes while lobular regions were HER2-
148 Enriched (but stained negative for HER2 IHC – Supplementary Table S1A). MDLC-1 ductal and
149 lobular regions were both of luminal IMS, with the former being Luminal A and the latter being
150 Luminal B. Finally, in line with mRNA expression patterns, MDLC-3 ductal and lobular regions
151 showed stark IMS differences (former Luminal A and later Basal-Like). MDLC-3 ductal region was
152 the only TNBC/Basal-Like tumor (and had low *ESR1*, *PGR* and *ERBB2* mRNA expression –
153 Supplementary Fig. S1E). We further confirmed the TNBC status of MDLC-3 ductal regions using

154 ER and HER2 IHC (Supplementary Table S1A). Overall, our transcriptomic clustering and IMS
155 analysis suggest that ductal and lobular tumor regions within mDLC may have distinct
156 transcriptomes and intrinsic subtypes.

157 **Differential Transcriptomic Features and Comparison with Pure ILC and IDC-NST**

158 To investigate global transcriptomic differences between ductal and lobular regions across all
159 cases, we performed differential gene expression analysis in a pan-patient manner. To avoid
160 biases caused by fundamental differences between ER+ and ER- disease, we excluded MDLC-3
161 ER-/TNBC ductal regions from this analysis and later downstream analyses (Supplementary Fig.
162 S2C). In total, we identified 168 significantly up-regulated and 198 significantly down-regulated
163 differentially expressed genes (DEGs) in the lobular compared to ductal regions across all cases
164 (Fig. 2B). These pan-patient DEGs showed strong overlap with patient specific DEGs
165 (Supplementary Fig. S2A,B,C) indicating that our pan-patient analysis captured most if not all
166 strong global differences between ductal and lobular tumor regions.

167 To assess transcriptomic similarity of mDLC ductal and lobular regions to pure counterparts, i.e.,
168 IDC-NST and ILC, we compared mDLC ductal vs. lobular region DEGs with those from the
169 comparison of TCGA ER+ IDC-NST (N=327) vs ILC (N=113), respectively (Fig. 2C). We found *KLK11,*
170 *KLK10, NRAP, SHROOM1, BTG2,* and *PDK4* were upregulated, while *CDH1*, *DCD, SERPINA1*, and
171 *CPB1* were downregulated in both comparisons (i.e., mDLC lobular vs ductal tumor regions and
172 ILC vs IDC-NST tumors). This overlap confirmed the well-known (i.e., down-regulation of *CDH1*)
173 markers of the lobular phenotype as well as potential novel markers.

174 **Differential Enrichment of ER and MYC Signatures & Recurring Biological Themes**

To understand the distinct biology of ductal and lobular regions, we scored each DSP region for hallmark signatures[45]. Twenty signatures were differentially enriched between ductal and lobular regions with p-value ≤ 0.05 (Fig. 2D, Supplementary Table S6). Findings for several signatures, including Kras Signaling Up/Dn, Estrogen Response Early/Late, Tnfa Signaling, and Hypoxia in the lobular regions, and Myc Targets V1, Protein Secretion and Adherens Junction in ductal regions, were largely recapitulated in MDLC-1 scRNAseq data (Supplementary Fig. S6D). In line with differential enrichment of Estrogen Response and Myc Target signatures, our transcription factor (TF) signature analysis revealed enrichment of *ESR1* TF signatures in lobular and *MYC* TF signatures in ductal regions (Supplementary Fig. S3). In summary, our findings show enrichment of distinct oncogenic signatures in ductal vs. lobular regions.

To determine recurring biological themes, we expanded our differential enrichment analysis to include all GO[46], REACTOME[47] and KEGG[48] genesets. Signatures differentially enriched between ductal and lobular regions with p-value ≤ 0.05 were further assessed for robustness against background permutations. Robust signatures were grouped into signature clusters based on similarity of overlapping genes. This was done separately for signatures enriched in ductal and lobular regions. All signature clusters were further grouped into broad biological themes based on the underlying biological terms (Fig. 2E, left panel). The mean score of all signature clusters in ductal and lobular regions is shown in Fig. 2E, right panel. Lobular regions were enriched for TP53 & senescence, collagen & extracellular matrix, MAPK/ERK targets (in line with KRAS signatures shown in Fig. 2D) among other signatures. In contrast, ductal regions were enriched in double stranded break & homologous repair, mTOR signaling (in line with Mtorc1/Mtor signatures

196 shown in Fig. 2D) among other signatures (Supplementary Table S7). Additionally, the expression
197 of senescence or cell cycle arrest genes (*CDKN1A/2B*) aligned with L2, collagen genes
198 (*COL4A1/4/5*) aligned with L5, and ERK/MAPK target genes (*DUSP4/6*) aligned with L9 signature
199 clusters were upregulated in lobular regions (Supplementary Fig. S4A,B,D). Enrichment of both
200 ERK/MAPK (L9) and KRAS signatures (from hallmark analysis) indicate higher activity of
201 KRAS/ERK/MAPK signaling in lobular regions, whereas enrichment of mTOR (D5) and
202 Mtorc1/Mtor signaling (from hallmark analysis) indicate higher activity of mTOR signaling in
203 ductal regions. In summary, we found differential enrichment of various cell cycle, immune,
204 collagen & ECM, metabolism, and oncogenic signatures between ductal vs. lobular regions.

205 **Genomic Landscape and Clinically Relevant Genomic Alterations**

206 To explore the genomic landscape of ductal and lobular regions, we employed the FDA-approved
207 targeted MSK-IMPACT panel. We micro-dissected the ductal and lobular tumor regions from FFPE
208 blocks of each case and sequenced them at a median depth of 416x (range 287–563)
209 (Supplementary Fig. S5A). In all cases, at least one pathogenic mutation was detected in known
210 breast cancer driver genes, including *CDH1, PIK3CA, TP53, GATA3, KMT2C, MAPK31, ARID1A,* and
211 *CBFB*, in both ductal and lobular regions, as depicted in Fig. 3A. Furthermore, all pathogenic
212 mutations had a high cancer cell fraction (Supplementary Fig. S5B).

213 Loss of E-cadherin is an established driver of lobular tumorigenesis[49]. Typically, it results from
214 biallelic *CDH1* inactivation, through a combination of truncating mutation and loss of
215 heterozygosity (LOH)[27]. All lobular regions exhibited loss of E-cadherin, with both MDLC-1 and
216 MDLC-3 harboring *CDH1* truncating mutations and LOH (Fig. 3B; Fig. 1E; Supplementary Fig. S1E).

The lobular region of MDLC-2 did not have *CDH1* genomic alterations but showed epigenetic inactivation via methylation of its promoter. A putative passenger mutation in *CDH1* was also observed in the MDLC-3 ductal region, which had no effect on mRNA or E-cadherin levels (Fig. 1E; Supplementary Fig. S1E). The loss of E-cadherin is consistent with the downstream down-regulation of Adherens Junction signatures in all lobular regions (Fig. 2D). Hotspot *PIK3CA* mutations, which are early oncogenic driver events frequently observed in ER+ BC[50], were present in all cases except MDLC-3. The MDLC-1 ductal region had mutations in *GATA3* (critical transcriptional binding partner of ERalpha[51]) and *CBFB* (forms complex with *RUNX1* to suppress NOTCH signaling[52]). The MDLC-3 ductal region had loss of *TP53*, an event associated with more aggressive types of breast cancer like basal/TNBC[53] and consistent with its basal-like intrinsic subtype. MDLC-2 ductal region had truncating mutation in *KMT2C*, an important regulator of ER alpha activity[54]. MDLC-3 lobular region had mutations in *ATRX* and *ARID1A,* two chromatin remodeling and DNA repair genes[55]. In addition, while MDLC-1 and MDLC-3 ductal and lobular regions did not share any somatic clonal mutations, MDLC-2 ductal and lobular regions shared several somatic clonal mutations in *PIK3CA* and *MAPK31* genes indicating shared tumor origin.

To investigate the copy number (CN) landscape of ductal and lobular regions, we performed CN analysis using FACETS[56] (Fig. 3B). All regions exhibited breast cancer characteristic chromosome 1q gains and 16q losses[53]. Overall, ductal tumor regions showed more frequent aneuploidy events than lobular tumor regions. MDLC-3 ductal region showed the most aberrant CN profile consistent with its basal/TNBC etiology[53]. Moreover, chromosome 22 aneuploidy was only

observed in ductal tumor regions. Notably, both histologic regions of MDLC-3 and ductal region of MDLC-2 had *NOTCH2* gains or amplifications (Supplementary Fig. S5C).

Mutational Processes Driving Tumor Evolution

To determine the mutational processes underlying the evolution of ductal and lobular tumor regions within mDLC, we performed mutational signature analysis of all cases (Fig. 3C). Both histologic regions in MDLC-2 were associated with an "aging" signature. In MDLC-3, ductal region was associated with homologous repair deficiency (HDR) while the lobular regions with APOBEC signature. Tumors with an APOBEC signatures have a higher frequency of mutations in chromatin remodeling and DNA repair genes[57], as seen in MDLC-3 lobular region. We did not identify any signatures for MDLC-1 ductal and lobular regions. The putative evolution of each mDLC case and its histologic region based upon the mutations, *CDH1* alterations and mutational signatures is shown in Fig. 3D. Notably, the MDLC-2 ductal and lobular regions not only shared clonal pathogenic (*PIK3CA*) and passenger (*MST1R* and *MAP3K1*) mutations but also the "aging" mutational signature. Loss of function *CDH1* alterations were hallmark of all lobular regions across cases.

Single-Cell RNA-Sequencing and Identification of Ductal and Lobular Populations

To explore the heterogeneity of mDLC at a single-cell level, we performed scRNAseq sequencing of a fresh tumor specimen from MDLC-1. The resulting scRNAseq comprised of 4,671 cells and had sequencing saturation, reads in cell and median genes per cell as shown in Supplementary Fig. S6A. Clustering revealed two transcriptionally distinct tumor populations; however, we were unable to annotate these populations as ductal and lobular tumors using *CDH1* mRNA (Fig. 4A).

Notably, while the lobular regions showed loss of E-cadherin protein (Fig. 1G), the *CDH1* p.Q23* mutation in MDLC-1 (Fig. 3A) didn't alter *CDH1* mRNA levels (Supplementary Fig. S1E). Therefore, we derived ductal and lobular transcriptome signatures (Supplementary Table S5) from MDLC-1 DSP dataset and used these signatures to score each single cell in MDLC-1 scRNAseq dataset. Using this deconvolution approach, we successfully annotated ductal and lobular tumor populations in the scRNAseq dataset (Fig. 4B). There was significant overlap of ductal vs. lobular DEGs between scRNAseq and DSP datasets (Supplementary Fig. S6B,C). Differential enrichment of several hallmark signatures and recurring biological themes in ductal and lobular regions from DSP data was recapitulated in our scRNAseq data (Supplementary Fig. S7A,C). Notably, we saw enrichment of Estrogen and senescence signatures in lobular and Myc signature in ductal tumor cells in both DSP and scRNAseq datasets.

Single-Cell Heterogeneity and Mapping of Single-Cells to Spatial Regions

To investigate single-cell heterogeneity of ductal and lobular populations, we increased resolution of clustering to identify sub-clusters. Each sub-cluster had unique marker genes (Fig. 4C) and several of these also showed differential enrichment of hallmark signatures and recurring biological theme clusters (Supplementary Fig. S7B,D), indicating intra-tumor heterogeneity within ductal and lobular tumor populations. To investigate whether single-cell transcriptomic heterogeneity was associated with spatial heterogeneity, we mapped scRNAseq sub-clusters to DSP regions. To assess similarity between each region and sub-cluster, we scored all regions for sub-cluster marker genesets using GSVA (Fig. 4D). Each region was mapped to a sub-cluster for which it had most similarity (i.e., highest GSVA score) (Fig. 4E). The top five marker genes of each

scRNAseq sub-cluster (Supplementary Fig. S6D) are shown beside each sub-cluster and spatial region link. These findings perhaps suggest that the single-cells in each sub-cluster came from a spatially distinct niche in the tumor.

Discussion

Despite an increasing incidence of mDLC[29,30], this special subtype of breast cancer remains poorly understood, with limited knowledge about its overall biology and that of its underlying ductal and lobular tumor regions, as well as their clinical implications.

Spatially resolved and single-cell profiling techniques have revolutionized our understanding of physiological and pathological processes and tissue architecture[58]. Efforts such as Human Cell Atlas (HCA)[59] and those from other groups have successfully uncovered the major cell types and their spatial organization in both normal breast tissue[60,61] and breast cancer[62]. Spatial and single-cell profiling of primary breast cancer subtypes and metastatic disease have been instrumental in identifying novel molecular features and their prognostic value[63–67]. However, to date genome-wide spatial and single-cell investigation of mDLC has not been reported. To address this gap, we employed a state-of-the-art methodology, comprising of spatially resolved transcriptomics, genomics, and single-cell profiling to investigate the biology of individual tumor regions within mDLC of "collision" type. Our study confirmed various previously reported observations of genetic inactivation of *CDH1* and concomitant loss of E-cadherin in lobular regions[31–33,68] and the presence of distinct driver alterations in individual tumor regions[33,68]. Moreover, we also uncovered novel findings that highlight the vast heterogeneity within mDLC, several of which were indicative of distinct prognosis. Ductal and lobular tumor regions had distinct biological signatures, in particular senescence, ER and *MYC* signaling, and intrinsic molecular subtypes (IMS). These distinctions were most prominent in sample MDLC-3, which was clinically reported as ER+ tumor but molecular profiling revealed that the underlying ductal region was ER-/TNBC

with basal-like IMS while the lobular region was ER+ with luminal-A IMS. Notably, both ER- status and basal-like IMS are associated with worse prognosis and outcome than ER+ and luminal IMS[69,70]. This patient had brain and lung metastasis, both of which were also ER-, possibly indicating progression of the primary ER- ductal tumor. This observation is clinically significant, indicating that individual tumor regions within mDLC may have distinct clinical and biological features and that one may pose higher recurrence risk than the other.

Another notable finding was enrichment of senescence and ER signaling signatures in lobular while *MYC* signatures in ductal tumor regions. Further analysis at single-cell level revealed that these signatures were enriched in only one lobular subcluster (L2), highlighting molecular heterogeneity even within individual histologically distinct tumor regions. Most patients with ILC are strongly ER+ and respond well to endocrine therapies, while they are less proliferative and respond poorly to chemotherapy[14,20,27,71,72]. Whether this is also true for lobular regions within mDLC is an important question and must be further investigated. Perhaps, future trials can study whether patients with predominantly ductal vs. lobular mDLC respond differently to standard of care endocrine and chemotherapies. However, this will be difficult to do as frequency of mDLC cases is low and a specific trial dedicated to patients with this disease may not be feasible.

The presence of distinct clinically actionable alterations in individual tumor regions within mDLC is a clinically important observation. We show that these alterations may emerge via common (Aging in MDLC-2) or distinct (APOBEC or HRD in MDLC-3) mutational processes. Tumor regions with distinct alterations can possibly complicate patient prognosis and clinical management. Alterations in components of ER signaling (such as *GATA3, KMT2C*) as well as Notch signaling

324 (*CBFB*, *NOTCH2*) can lead to endocrine resistance[73–75], while alterations in DNA repair response
325 genes (*ARID1A*, *ATRX*) may confer increased sensitivity to chemotherapy and other DNA repair
326 pathway targeting drugs including PARP inhibitors[76,77]. Treatment regimens decisions for patients
327 with mDLC can greatly benefit from considering the distinct alterations in individual tumor
328 regions to avoid drug resistance by rational selection of therapies.

329 For a long time, it was unclear whether ductal and lobular regions within mDLC share any
330 molecular similarity with their pure counterparts (i.e., ILC and IDC-NST tumors). In our study, we
331 compared the molecular features of individual tumor regions within mDLC with their pure
332 counterparts in the TCGA cohort[27] and discovered a set of shared markers of lobular phenotype.
333 One of these marker genes was *CDH1*, whose inactivation drives lobular tumorigenesis[49]. This
334 primarily occurs via genetic alterations[27] which was the case in lobular regions of MDLC-1 and
335 MDLC-3. However, in lobular regions of MDLC-2, *CDH1* promoter methylation was observed,
336 indicating an alternative but less studied route of lobular tumor formation via epigenetic
337 inactivation. This is an intriguing observation, suggesting that the pathogenesis of lobular regions
338 within mDLC maybe more complex and diverse than previously thought[6,68,78–80]. Our expression
339 analysis of various previously reported[81] epithelial to mesenchymal (EMT) markers
340 (Supplementary Fig. S1F) excluded the role of EMT in driving this event.

341 A recent study revealed the synthetic lethality in E-cadherin deficient breast cancers with
342 inhibition of *ROS1*, a tyrosine kinase[82]. The ongoing ROSALINE trial is investigating efficacy of
343 *ROS1* inhibitors in early setting of ER+ ILC disease. If successful, future studies can assess the
344 value of *ROS1* inhibitors in treating patients with predominantly lobular mDLC disease. Additional

345 studies are also warranted to investigate whether E-cadherin deficient tumors with distinct
346 etiology, such as *CDH1* epigenetic or genetic inactivation, have distinct biology potentially
347 associated with differential treatment response.

348 Although our study presents a unique and novel analysis of mDLC of "collision" type, it has some
349 limitations, including small sample size and a lack of analysis of other subtypes (such as lobular-
350 like IDC-NST[83] and intermixed/intermingled mDLC[68]) and tumor microenvironment of individual
351 tumor regions within mDLC. Future studies will be necessary to validate our observations in larger
352 and more diverse cohorts of mDLC. Generating a comprehensive mDLC cohort for future studies
353 may not be an easy task, given the challenges associated with the diagnosis of this mixed entity.
354 However, the use of E-cadherin IHC in histological assessments and evaluation by a panel of
355 pathologists can ensure the generation of a high-confidence and well-annotated mDLC cohort
356 for future studies. Moreover, the application of digital pathology and artificial intelligence will
357 make this more feasible[84]. These tools will not only improve diagnostic accuracy[85] but will also
358 allow scalable annotation of ductal and lobular tumor regions across heterogenous tumor
359 samples[86].

360 In summary, our study provides new insights into the molecular heterogeneity of mDLC and its
361 underlying ductal and lobular tumor regions. This is the first report on genome-wide spatially
362 resolved and single-cell molecular profiling of mDLC. We discovered distinct biological signatures
363 and intrinsic molecular subtypes between these regions that may have important implications
364 for patient prognosis and clinical management. Our findings also highlight the need for
365 comprehensive histopathological and molecular profiling of individual tumor regions within

mDLC to better understand its progression and response to standard of care hormone and cytotoxic therapies.

368 ## Methods

369 **Sample Collection**

370 Institutional review board approval was obtained from the University of Pittsburgh prior to
371 initiation of the study. Patients diagnosed with "mixed invasive ductal and lobular" were
372 identified from the UPMC Breast Cancer Registry and Formalin-Fixed Paraffin-Embedded (FFPE)
373 blocks requested from Pitt Biospecimen Core. Four-um-thick FFPE sections were used for H&E,
374 ER-alpha and E-cadherin IHC staining. A panel of pathologists reviewed the H&E and E-cadherin
375 staining to confirm mDLC diagnosis in line with recent WHO guidelines (10-90% of ILC and at least
376 10% IDC-NST). For our pilot study, we only selected mDLC cases amenable for multi-omic profiling
377 i.e., those with good separation of ductal and lobular tumor regions to avoid spill over and
378 contamination of individual ductal and lobular tumor regions by neighboring lobular and ductal
379 tumor cells, respectively. Hence, we selected three "collision" type mDLC cases that showed both
380 clear separation of ductal and lobular tumor regions along with some intermixed regions. These
381 included cases MDLC-1, MDLC-2 & MDLC-3 (clinical features and pathology review notes are
382 shown in Supplementary Table S1A & S1B). All cases underwent NanoString digital spatial, MSK-
383 IMPACT mutation and *CDH1* promoter methylation profiling. Fresh tumor was only available for
384 MDLC-1 and was utilized for single-cell RNAseq. See details in Supplementary Methods.

385 **Digital Spatial Profiling (DSP)**

386 DSP was performed by NanoString GeoMX as described previously[87]. Briefly, five-µm-thick FFPE
387 tumor sections were mounted on single positively charged slide. Slides underwent
388 deparaffinization, rehydration, heat-induced epitope retrieval, and enzymatic digestion.

389 Oligonucleotide probe mix from whole-transcriptome atlas (WTA) panel were hybridized and
390 incubated overnight. The slide was blocked and incubated with fluorescent antibodies against
391 morphology markers and DNA dye (Syto83 dye; Invitrogen Cat # S11364) for 1 hour. Morphology
392 markers included E-cadherin (BD Pharmingen Cat# 560062), Pan-cytokeratin (Novus Cat# NBP2-
393 33200AF488) and Vimentin (Santa Cruz Cat# sc-373717 AF594). Finally, the slide was loaded into
394 the GeoMx platform and scanned for an immunofluorescent signal. Together with the aid of H&E
395 and morphology marker stains, our panel of pathologist selected 26 rectangle ROIs (12 lobular
396 ROIs, 11 ductal ROIs and 3 mixed ROIs) with an area of 518,100 μm^2. To profile ductal and lobular
397 cells separately the following segmentation approach was used; 1) ductal cells a E-cadherin +ive
398 & Pan- cytokeratin +ive, and 2) lobular cells a E-cadherin -ive & Pan- cytokeratin +ive. Above
399 segmentation resulted in total of 29 areas (14 ductal and 15 lobular). UV light was directed at
400 each segmented region to release the oligonucleotides that were collected and then sequenced
401 using Illumina NextSeq 2000. The resulting FASTQ files were processed using GeoMX NGS
402 pipeline 2.3.4 which provided the count data for all target probe across profiled regions. All 29
403 profiled regions had high sequencing saturation (> 94%) and low signal-to-noise ratio (Q3
404 count/NegProbe count ≥ 1) (Supplementary Fig. S1A-C; Supplementary Table S2,S3). Further
405 downstream analysis is described in the Supplementary Methods.

406 **MSK-IMPACT Targeted Next Generation Sequencing**

407 Eight-µm-thick sections from representative FFPE tumor and matched normal tissue sections
408 from MDLC-3, MDLC-2 & MDLC-1 were stained with nuclear fast red and microdissected using a
409 sterile needle under a stereomicroscope (Olympus SZ61) to enrich tumor content, as previously

410 described[88,89]. Histologically distinct tumor components were microdissected separately.
411 Genomic DNA of each component and of matched normal tissue was extracted using the DNeasy
412 Blood and Tissue Kit (Qiagen) according to manufacturers' instructions. Tumor and normal DNA
413 from each case were subjected to massively parallel sequencing using the Food and Drug
414 Administration (FDA) approved Memorial Sloan Kettering Integrated Mutation Profiling of
415 Actionable Cancer Targets (MSK-IMPACT) multigene panel targeting all coding regions of 515
416 cancer-related genes as previously described[90–92]. Somatic alterations were identified as
417 previously described[93,94] (Supplementary Table S8). The median depth of coverage of tumor and
418 normal samples was 416x (range 287–563) and 210x (range 175-217), respectively
419 (Supplementary Fig. S5A). In brief, reads were aligned to the reference human genome GRCh37
420 using the BWA v0.7.15[95]. Local realignment, duplicate removal and base quality recalibration
421 were performed using the GATK. V3.1.1[96]. Further downstream analysis is described in the
422 Supplementary Methods.

423 **Figures & Illustrations**

424 DSP spatial images were exported from Most bioinformatic analysis visualizations were
425 generated using R. These visualizations were aesthetically improved in power point to produce
426 the final figures. Illustrations were prepared using BioRender.com.

427 **Data Availability**

428 Data generated in this study is shared and can be included in the Supplementary Data and GitHub.
429 R code for data analysis can be accessed at
430 https://github.com/osamashiraz/mDLC_Spatial_Analysis.

Authors' Disclosures

PCL has an equity interest in Amgen (outside the submitted work). No disclosures were reported by other authors.

Authors' Contributions

O.S. Shah: Conceptualization, data curation, software, formal analysis, investigation, visualization, methodology, project administration, writing–original draft, writing–review and editing. **A. Nasrazadani:** resources, funding acquisition, writing-review and editing. **J.M. Atkinson:** resources, supervision, project administration, writing–review and editing. **J. Foldi:** resources, investigation, data curation, writing–review and editing. **C.G. Kleer:** investigation, data curation, writing–review and editing. **P.F. McAuliffe:** investigation, resources, data curation, writing–review and editing. **E.M. da Silva:** investigation, resources, data curation, software, formal analysis, writing–review and editing. **P. Selenica:** investigation, resources, data curation, software, formal analysis, writing–review and editing. **H. Dopeso:** investigation, resources, data curation, writing–review and editing. **F. Pareja:** investigation, resources, data curation, writing–review and editing. **D. Mandelker:** investigation, resources, data curation, writing–review and editing. **B. Weigelt:** conceptualization, investigation, methodology, resources, writing–review and editing. **J.S. Reis-Filho:** conceptualization, investigation, methodology, resources, writing–review and editing. **R. Bhargava:** conceptualization, investigation, resources, data curation, methodology, data curation, writing–review and editing. **P.C. Lucas:** conceptualization, investigation, resources, data curation, methodology, data curation, writing–review and editing. **A.V. Lee:** conceptualization, resources, methodology, supervision, funding acquisition, project administration, writing–review and editing. **S. Oesterreich:** conceptualization, resources, methodology, supervision, funding acquisition, project administration, writing–review and editing.

Acknowledgments

We would also like to thank NanoString DSP Technology Access Program for providing early access to their whole transcriptome spatial technology, Pitt Biospecimen Core at University of Pittsburgh for providing access to valuable clinical specimens and technical support, Pitt Genomics Research Core and UPMC Genome Center for technical support in preparing scRNAseq libraries and sequencing, and Ms. Morgan DeBerry, HTL(ASCP)CM, QIHCCM for excellent technical assistance in tissue sectioning, staining and other logistics. This work was primarily supported by Dynami and BCRF grants to **S. Oesterreich** and in part by various other grants including the ASCO Gianni Bonadonna Breast Cancer Research Fellowship grant to **A. Nasrazadani** and Conquer Cancer ASCO Young Investigator Award to **J. Foldi**.

Figure Legends

Figure 1. Digital Spatial Profiling of mDLC Ductal and Lobular Tumor Regions. (A) Top panel shows clinical timelines of the studied cases including the time of core biopsies, surgical interventions, treatments, metastasis and last known vital status. The source of the tumor tissue used in this study is highlighted with * in red color. The bottom panels show high (40X) magnification H&E and Ecad/p120 IHC images highlighting histomorphic and E-cadherin features of ductal and lobular regions across each case. (B) E-cadherin and Pan-CK immunofluorescence staining of a representative case (MDLC-3). Selected regions of interests (ROIs) are shown with dotted blue (for ductal) and red (for lobular). (C) Segmentation of ductal and lobular cells using E-cadherin and Pan-CK staining masks. (D) Segmented areas containing only ductal or lobular tumor cells defined using ductal and lobular masks illustrated in panel C. (E) E-cadherin staining intensity in representative ductal and lobular regions profiled across cases.

Figure 2. Molecular Subtypes and Distinct Biological Signatures of Ductal and Lobular Tumor Regions. (A) Profiled ductal and lobular tumor regions separated by consensus clusters. All regions are annotated by patients, histology, and consensus clusters. Gene expression heatmap shows top variable genes and followed by PAM50 scores for each subtype across ductal and lobular regions. (B) Differentially expressed genes (DEGs) between ER+ ductal and lobular regions. The top panel shows DEG heatmap, while bottom panel shows volcano plot along with number of significantly upregulated (N=168) and downregulated (N=198) DEGs in lobular vs ductal regions. (C) Overlap of ductal and lobular region DEGs with TCGA ILC vs IDC-NST DEGs. (D) Differentially enriched cancer hallmark pathways. The heatmap shows GSVA scores of each

differentially enriched pathway in ductal vs lobular tumor regions. Pathways with bold red and blue names are the ones that also were significant in the scRNAseq dataset (Supplementary Fig. S7A). Enrichment score (ES) for a pathway shows mean differences of GSVA score for that pathway in lobular – ductal regions and -log10 of FDR-adjusted P-value (P-val) shows statistical significance of enrichment based on T test. (E) Recurrent biological themes in ductal and lobular tumor regions. The left panel shows the Jaccard similarity between all signatures. Signatures are grouped based on their Jaccard similarity into signature clusters. Each cluster is associated with a broad biological theme (shown in middle). The right panel shows the mean GSVA score of each signature cluster in ductal and lobular regions.

Figure 3. Overview of Genomic Alterations in Ductal and Lobular Tumor Regions. (A) Somatic mutations identified using MSK-IMPACT panel in ductal and lobular components across samples. Gene names are followed by amino acid change due to mutation. Genes in black font had somatic mutations in breast cancer driver genes while those in gray color had passenger/non-driver mutations. (B) Somatic copy number changes in ductal and lobular components across samples. For each case, genome-wide ductal and lobular copy number profiles are shown. Black line shows total copy number, red line shows minor allele copy number and off-white regions show aneuploidy (change in minor allele copy number including LOH). (C) Mutational signatures in MDLC-2 and MDCL-3 ductal and lobular tumor regions. Pie charts show percentage similarity of mutational patterns of each tumor component with established mutational patterns (associated with different means/definition). (D) Predicted disease evolution. Tumors with overlapping mutations were linked to common root node indicating common progenitor or precursor

neoplasm (N). Those without common root node likely indicate evolution from independent precursors. Key mutations and events (CDH1 promoter methylation and amplifications) are shown on the branches.

Figure 4: Single Cell Heterogeneity of Ductal and Lobular Tumor Populations. (A) Tumor populations in MDLC-1 scRNAseq dataset (left) and assessment of CDH1 expression in MDLC-1 scRNAseq dataset (middle and right plot). Statistical significance was evaluated using the T test. (B) Deconvolution of scRNAseq using DSP derived ductal and lobular signatures. GSVA scores for ductal and lobular signatures are shown on the right panel. (C) Sub-clustering and identification of ductal and lobular sub-populations (left) with unique marker genes (right). (D) Scoring spatial regions using GSVA of sub-cluster marker genes. (E) Mapping of single cell populations to spatial regions based on GSVA scores in D.

Supplementary Figure Legends

Supplementary Figure S1: Digital Spatial Profiling RNAseq Dataset Quality Control. (A) Scatter plot showing sequencing saturation (y-axis) and area of interest (AOI) surface area (mm2) across cases. Dashed red lines show the quality control (QC) cutoffs (sequencing saturation >50% and area > 6000mm2) for selecting high quality samples. (B) Overview of signal (Q3-normalized counts) to noise (negative probe counts). Dashed red line shows cutoff i.e., signal > noise. (C) Evaluation of Q3 normalized counts (of 1000 randomly sampled genes) across profiled regions to identify samples with low quality data showing count artifacts. (D) tSNE plot showing clustering of profiled samples that passed QC cutoffs. (E) CDH1, ESR1, ERBB2 and PGR gene expression in ductal vs lobular regions across the three profiled cases. Statistical significance was evaluated using the T test. (F) Expression of EMT marker genes in ductal and lobular tumor regions across each case. EMT marker genes were adapted from McCart Reed et al [33].

Supplementary Figure S2: Patient Wise Differential Analysis and Comparison with Pan-Patient Differential Analysis. Differentially expressed genes (DEGs) identified in ductal vs lobular in each patient; MDLC-1 (A), MDLC-2 (B) and MDLC-3 (C) and overlap of patient-wise DEGs with pan-patient (all patients combined) DEGs. Statistical significance of overlap between patient DEGs and pan-patient DEGs was test using overlap_stats tool (http://nemates.org/MA/progs/overlap_stats.html)**.** A representation score > 1 and $p < 0.05$ shows significantly strong overlap.

Supplementary Figure S3: Transcription Factor Enrichment Analysis using Pan-Patient Lobular vs Ductal DEGs. Lobular vs Ductal DEGs were separately input into https://maayanlab.cloud/X2K/

web portal to identify enriched transcription factors and kinases in lobular (left) and ductal (right) tumor regions. The top layer with blue nodes shows kinases, middle layer shows intermediate proteins and bottom layer with red nodes shows transcription factors. An image inset is shown highlighting MYC and ER signaling related transcription factors enriched in ductal and lobular tumor regions, respectively.

Supplementary Figure S4: Genes Associated with Key Differentially Enriched Biological Signatures. Select differentially expressed genes in various differentially enriched biological signature clusters between ductal vs. lobular tumor regions including (A) L2: TP53/Senescence, (B) L5: Collagen & ECM, (C) L7: Collagen metabolism, (D) L9: MAPK/ERK Targets, (E) D5: mTOR, (F) D4: Oxidative Stress, (G) D6: Acetyltransferase, (H) D7: Protein Maturation and (I) D8: Phosphatidylinositol. Statistical significance was evaluated using the T test.

Supplementary Figure S5: MSK-IMPACT Extended Results. (A) Tumor purity, sequencing coverage and ploidy of ductal and lobualr tumor regions across profiled cases. (B) Somatic mutations and their cancer cell fraction (CCF). High CCF indicate clonal mutations while low CCF indicates sub-clonal mutations. (C) Copy number of key breast cancer genes in ductal vs lobular regions across each case.

Supplementary Figure S6: Single-cell RNAseq DEG and Pathway Analysis of MDLC-1. (A) MDLC-1 single-cell RNAseq (scRNAseq) dataset quality control meterics from cell ranger software. (B) MDLC-1 scRNAseq lobular vs ductal DEG analysis. (C) Overlap of MDLC-1 lobular vs ductal DEGs between scRNseq and digital spatial profiling (DSP) datasets. Statistical significance of DEG overlap between two technologies was test using overlap_stats tool

561 (http://nemates.org/MA/progs/overlap_stats.html). A representation score > 1 and p < 0.05
562 shows significantly strong overlap. (D) Top five marker genes of each lobular and ductal sub-
563 cluster identified in Fig. 4C.

564 **Supplementary Figure S7: MDLC-1 Single-cell RNAseq Pathway Analysis.** (A) GSVA based
565 hallmark signature enrichment analysis in scRNAseq dataset. Enrichment score (ES) for a pathway
566 shows mean differences of GSVA score for that pathway in lobular – ductal regions and -log10 of
567 FDR-adjusted P-value (P-val) shows statistical significance of enrichment based on T test. (B)
568 Hallmark signature enrichment in ductal and lobular subclusters. (C) Recurrening biology themes
569 in ductal vs lobular cells in scRNAseq dataset. (D) Mean GSVA score for select differentially
570 enriched biology themes across sub-clusters.

References

1. Bray, F. *et al.* Global cancer statistics 2018: GLOBOCAN estimates of incidence and mortality worldwide for 36 cancers in 185 countries. **68**, 394–424 (2018).
2. Siegel, R. L., Miller, K. D., Wagle, N. S. & Jemal, A. Cancer statistics, 2023. *CA Cancer J Clin* **73**, 17–48 (2023).
3. Sledge, G. W., Chagpar, A. & Perou, C. Collective wisdom: lobular carcinoma of the breast. *Am Soc Clin Oncol Educ B* **35**, 18–21 (2016).
4. Reed, M. E. M. C., Kutasovic, J. R., Lakhani, S. R. & Simpson, P. T. Invasive lobular carcinoma of the breast: morphology, biomarkers and ’omics. **17**, 12 (2015).
5. Ciriello, G. *et al.* Comprehensive molecular portraits of invasive lobular breast cancer. *Cell* **163**, 506–519 (2015).
6. Reed, M. E. M. C., Kutasovic, J. R., Lakhani, S. R. & Simpson, P. T. Invasive lobular carcinoma of the breast: morphology, biomarkers and ’omics. **17**, 12 (2015).
7. Dabbs, D. J., Bhargava, R. & Chivukula, M. Lobular versus ductal breast neoplasms: the diagnostic utility of p120 catenin. *Am J Surg Pathol* **31**, 427–37 (2007).
8. Arpino, G. *et al.* Infiltrating lobular carcinoma of the breast: tumor characteristics and clinical outcome. **6**, (2004).
9. Oesterreich, S. *et al.* Clinicopathological Features and Outcomes Comparing Patients With Invasive Ductal and Lobular Breast Cancer. *J Natl Cancer Inst* **114**, 1511–1522 (2022).
10. Z, C. *et al.* Invasive lobular carcinoma of the breast: A special histological type compared with invasive ductal carcinoma. **12**, e0182397 (2017).
11. Yeatman, T. J. *et al.* Tumor biology of infiltrating lobular carcinoma. Implications for management. *Ann Surg* **222**, 549–559 (1995).
12. Helvie, M. A., Paramagul, C., Anderson, K. L. & Adler, D. D. Invasive lobular carcinoma. Imaging features and clinical detection. *Invest Radiol* **28**, 202–207 (1993).
13. Arpino, G. *et al.* Infiltrating lobular carcinoma of the breast: tumor characteristics and clinical outcome. **6**, (2004).
14. Oesterreich, S. *et al.* Clinicopathological Features and Outcomes Comparing Patients With Invasive Ductal and Lobular Breast Cancer. *J Natl Cancer Inst* **114**, 1511–1522 (2022).
15. Mathew, A. *et al.* Distinct Pattern of Metastases in Patients with Invasive Lobular Carcinoma of the Breast. *Geburtshilfe Frauenheilkd* (2017) doi:10.1055/s-0043-109374.
16. Lamovec, J. & Bračkko, M. Metastatic pattern of infiltrating lobular carcinoma of the breast: an autopsy study. **48**, 28–33 (1991).
17. Djerroudi, L., Cabel, L., Bidard, F. C. & Vincent-Salomon, A. Invasive Lobular Carcinoma of the Breast: Toward Tailoring Therapy? **114**, 1434–1436 (2022).

18. K, V. B. *et al.* Current and future diagnostic and treatment strategies for patients with invasive lobular breast cancer. *Annals of Oncology* **33**, 769–785 (2022).

19. Luveta, J., Parks, R. M., Heery, D. M., Cheung, K.-L. & Johnston, S. J. Invasive Lobular Breast Cancer as a Distinct Disease: Implications for Therapeutic Strategy. *Oncol Ther* **8**, 1–11 (2020).

20. K, V. B. *et al.* Current and future diagnostic and treatment strategies for patients with invasive lobular breast cancer. *Annals of Oncology* **33**, 769–785 (2022).

21. The 2019 World Health Organization classification of tumours of the breast - Tan - 2020 - Histopathology - Wiley Online Library.

22. Metzger-Filho, O. *et al. The diagnosis of mixed invasive ductal and lobular carcinoma (IDC-L) in clinical practice is often associated with uncertainty related to its prognosis and response to systemic therapies. With the increasing recognition of invasive lobular carc*. vol. 24 (Oxford University Press (OUP), 2019).

23. Zengel, B. *et al.* Comparison of the clinicopathological features of invasive ductal, invasive lobular, and mixed (invasive ductal + invasive lobular) carcinoma of the breast. *Breast Cancer* (2015) doi:10.1007/s12282-013-0489-8.

24. Xiao, Y. *et al.* Mixed invasive ductal and lobular carcinoma has distinct clinical features and predicts worse prognosis when stratified by estrogen receptor status. *Sci Rep* (2017) doi:10.1038/s41598-017-10789-x.

25. Duraker, N., Hot, S., Akan, A. & Ozay Nayir, P. A Comparison of the Clinicopathological Features, Metastasis Sites and Survival Outcomes of Invasive Lobular, Invasive Ductal and Mixed Invasive Ductal and Lobular Breast Carcinoma. *Eur J Breast Health* **16**, 22–31 (2020).

26. Nasrazadani, A. *et al.* Mixed invasive ductal lobular carcinoma is clinically and pathologically more similar to invasive lobular than ductal carcinoma. *British Journal of Cancer 2023* 1–10 (2023) doi:10.1038/s41416-022-02131-8.

27. Ciriello, G. *et al.* Comprehensive molecular portraits of invasive lobular breast cancer. *Cell* **163**, 506–519 (2015).

28. Nasrazadani, A. *et al.* Mixed invasive ductal lobular carcinoma is clinically and pathologically more similar to invasive lobular than ductal carcinoma. *British Journal of Cancer 2023* 1–10 (2023) doi:10.1038/s41416-022-02131-8.

29. Li, C. I., Anderson, B. O., Daling, J. R. & Moe, R. E. Trends in Incidence Rates of Invasive Lobular and Ductal Breast Carcinoma. *J Am Med Assoc* (2003) doi:10.1001/jama.289.11.1421.

30. Suryadevara, A., Paruchuri, L. P., Banisaeed, N., Dunnington, G. & Rao, K. A. The clinical behavior of mixed ductal/lobular carcinoma of the breast: A clinicopathologic analysis. *World J Surg Oncol* (2010) doi:10.1186/1477-7819-8-51.

31. Rakha, E. A. *et al.* The biological and clinical characteristics of breast carcinoma with mixed ductal and lobular morphology. *Breast Cancer Res Treat* (2009) doi:10.1007/s10549-008-0007-4.

32. Acs, G., Lawton, T. J., Rebbeck, T. R., LiVolsi, V. A. & Zhang, P. J. Differential Expression of E-Cadherin in Lobular and Ductal Neoplasms of the Breast and Its Biologic and Diagnostic Implications. *Am J Clin Pathol* (2001) doi:10.1309/FDHX-L92R-BATQ-2GE0.

33. McCart Reed, A. E. *et al.* Mixed ductal-lobular carcinomas: evidence for progression from ductal to lobular morphology. *Journal of Pathology* (2018) doi:10.1002/path.5040.

34. Metzger-Filho, O. *et al.* Mixed Invasive Ductal and Lobular Carcinoma of the Breast: Prognosis and the Importance of Histologic Grade. *Oncologist* **24**, (2019).

35. Zhao, H. The prognosis of invasive ductal carcinoma, lobular carcinoma and mixed ductal and lobular carcinoma according to molecular subtypes of the breast. *Breast Cancer* **28**, 187–195 (2021).

36. Arps, D. P., Healy, P., Zhao, L., Kleer, C. G. & Pang, J. C. Invasive ductal carcinoma with lobular features: a comparison study to invasive ductal and invasive lobular carcinomas of the breast. *Breast Cancer Res Treat* **138**, 719 (2013).

37. M, C. *et al.* Lobular breast cancer: Histomorphology and different concepts of a special spectrum of tumors. **13**, 3695 (2021).

38. Christgen, M., Kandt, L. D., Antonopoulos, W. & al., et. Inter-observer agreement for the histological diagnosis of invasive lobular breast carcinoma. *J Pathol Clin Res* **8**, 191–205 (2022).

39. Z, C. *et al.* Invasive lobular carcinoma of the breast: A special histological type compared with invasive ductal carcinoma. **12**, e0182397 (2017).

40. Yeatman, T. J. *et al.* Tumor biology of infiltrating lobular carcinoma. Implications for management. *Ann Surg* **222**, 549–559 (1995).

41. Helvie, M. A., Paramagul, C., Anderson, K. L. & Adler, D. D. Invasive lobular carcinoma. Imaging features and clinical detection. *Invest Radiol* **28**, 202–207 (1993).

42. Mann, R. M. The effectiveness of MR imaging in the assessment of invasive lobular carcinoma of the breast. *Magn Reson Imaging Clin N Am* **18**, 259–276 (2010).

43. Christgen, M., Kandt, L. D., Antonopoulos, W. & al., et. Inter-observer agreement for the histological diagnosis of invasive lobular breast carcinoma. *J Pathol Clin Res* **8**, 191–205 (2022).

44. Pérez-Mies, B. *et al.* The Clonal Relationship Between the Ductal and Lobular Components of Mixed Ductal-Lobular Carcinomas Suggested a Ductal Origin in Most Tumors. *American Journal of Surgical Pathology* **46**, 1545–1553 (2022).

45. Liberzon, A. *et al.* The Molecular Signatures Database Hallmark Gene Set Collection. *Cell Syst* **1**, 417–425 (2015).

46. Carbon, S. *et al.* The Gene Ontology resource: enriching a GOld mine. *Nucleic Acids Res* **49**, D325–D334 (2021).

47. Gillespie, M. *et al.* The reactome pathway knowledgebase 2022. *Nucleic Acids Res* **50**, D687–D692 (2022).

48. Kanehisa, M., Furumichi, M., Sato, Y., Kawashima, M. & Ishiguro-Watanabe, M. KEGG for taxonomy-based analysis of pathways and genomes. *Nucleic Acids Res* **51**, D587–D592 (2023).

49. Cleton-Jansen, A. M. E-cadherin and loss of heterozygosity at chromosome 16 in breast carcinogenesis: different genetic pathways in ductal and lobular breast cancer? *Breast Cancer Res* **4**, 5–8 (2002).

50. André, F. *et al.* Alpelisib for PIK3CA -Mutated, Hormone Receptor–Positive Advanced Breast Cancer . *New England Journal of Medicine* **380**, 1929–1940 (2019).

51. Theodorou, V., Stark, R., Menon, S. & Carroll, J. S. GATA3 acts upstream of FOXA1 in mediating ESR1 binding by shaping enhancer accessibility. *Genome Res* **23**, 12 (2013).

52. Malik, N. *et al.* The transcription factor CBFB suppresses breast cancer through orchestrating translation and transcription. *Nature Communications 2019 10:1* **10**, 1–15 (2019).

53. Comprehensive molecular portraits of human breast tumours. *Nature* **490**, (2012).

54. Gala, K. *et al.* KMT2C mediates the estrogen dependence of breast cancer through regulation of ERα enhancer function. *Oncogene 2018 37:34* **37**, 4692–4710 (2018).

55. Glaser, A. P. *et al.* APOBEC-mediated mutagenesis in urothelial carcinoma is associated with improved survival, mutations in DNA damage response genes, and immune response. *Oncotarget* **9**, 4537–4548 (2017).

56. Shen, R. & Seshan, V. E. FACETS: allele-specific copy number and clonal heterogeneity analysis tool for high-throughput DNA sequencing. *Nucleic Acids Res* **44**, (2016).

57. Glaser, A. P. *et al.* APOBEC-mediated mutagenesis in urothelial carcinoma is associated with improved survival, mutations in DNA damage response genes, and immune response. *Oncotarget* **9**, 4537–4548 (2017).

58. Moffitt, J. R., Lundberg, E. & Heyn, H. The emerging landscape of spatial profiling technologies. *Nature Reviews Genetics 2022 23:12* **23**, 741–759 (2022).

59. van Amerongen, R. Behind the Scenes of the Human Breast Cell Atlas Project. *J Mammary Gland Biol Neoplasia* **26**, 67 (2021).

60. Nguyen, Q. H. *et al.* Profiling human breast epithelial cells using single cell RNA sequencing identifies cell diversity. *Nat Commun* (2018) doi:10.1038/s41467-018-04334-1.

61. Gray, G. K. *et al.* A human breast atlas integrating single-cell proteomics and transcriptomics. *Dev Cell* **57**, 1400-1420.e7 (2022).

62. Wu, S. Z. *et al.* A single-cell and spatially resolved atlas of human breast cancers. *Nature Genetics 2021 53:9* **53**, 1334–1347 (2021).

63. Sun, H. *et al.* The relevance between hypoxia-dependent spatial transcriptomics and the prognosis and efficacy of immunotherapy in claudin-low breast cancer. *Front Immunol* **13**, 7828 (2023).

64. Bassiouni, R. *et al.* Spatial Transcriptomic Analysis of a Diverse Patient Cohort Reveals a Conserved Architecture in Triple-Negative Breast Cancer. *Cancer Res* **83**, 34–48 (2023).

65. Johnson, B. E. *et al.* An omic and multidimensional spatial atlas from serial biopsies of an evolving metastatic breast cancer. *Cell Rep Med* **3**, 100525 (2022).

66. Kulasinghe, A. *et al.* Spatial Profiling Identifies Prognostic Features of Response to Adjuvant Therapy in Triple Negative Breast Cancer (TNBC). *Front Oncol* **11**, 1 (2021).

67. Andersson, A. *et al.* Spatial deconvolution of HER2-positive breast cancer delineates tumor-associated cell type interactions. *Nature Communications 2021 12:1* **12**, 1–14 (2021).

68. Pérez-Mies, B. *et al.* The Clonal Relationship Between the Ductal and Lobular Components of Mixed Ductal-Lobular Carcinomas Suggested a Ductal Origin in Most Tumors. *American Journal of Surgical Pathology* **46**, 1545–1553 (2022).

69. Badve, S. *et al.* Basal-like and triple-negative breast cancers: a critical review with an emphasis on the implications for pathologists and oncologists. *Modern Pathology* **24**, 157–167 (2011).

70. Perou, C. M. Molecular Stratification of Triple-Negative Breast Cancers. *Oncologist* **16**, 61–70 (2011).

71. Michaut, M. *et al.* Integration of genomic, transcriptomic and proteomic data identifies two biologically distinct subtypes of invasive lobular breast cancer. *Sci Rep* (2016) doi:10.1038/srep18517.

72. Djerroudi, L., Cabel, L., Bidard, F. C. & Vincent-Salomon, A. Invasive Lobular Carcinoma of the Breast: Toward Tailoring Therapy? **114**, 1434–1436 (2022).

73. Azim, H. A., Nguyen, B., Brohée, S., Zoppoli, G. & Sotiriou, C. Genomic aberrations in young and elderly breast cancer patients. *BMC Med* **13**, 1–7 (2015).

74. Afzaljavan, F., Sadr, A. S., Savas, S. & Pasdar, A. GATA3 somatic mutations are associated with clinicopathological features and expression profile in TCGA breast cancer patients. *Scientific Reports 2021 11:1* **11**, 1–13 (2021).

75. BeLow, M. & Osipo, C. Notch Signaling in Breast Cancer: A Role in Drug Resistance. *Cells 2020, Vol. 9, Page 2204* **9**, 2204 (2020).

76. Hopkins, J. L., Lan, L. & Zou, L. DNA repair defects in cancer and therapeutic opportunities. *Genes Dev* **36**, 278 (2022).

77. Voutsadakis, I. A. & Stravodimou, A. Homologous Recombination Defects and Mutations in DNA Damage Response (DDR) Genes Besides BRCA1 and BRCA2 as Breast Cancer Biomarkers for PARP Inhibitors and Other DDR Targeting Therapies. *Anticancer Res* **43**, 967–981 (2023).

78. McCart Reed, A. E. *et al.* Mixed ductal-lobular carcinomas: evidence for progression from ductal to lobular morphology. *Journal of Pathology* (2018) doi:10.1002/path.5040.

79. Kutasovic, J. R., McCart Reed, A. E., Sokolova, A., Lakhani, S. R. & Simpson, P. T. Morphologic and genomic heterogeneity in the evolution and progression of breast cancer. *Cancers* vol. 12 Preprint at https://doi.org/10.3390/cancers12040848 (2020).

80. Ciriello, G. *et al.* Comprehensive Molecular Portraits of Invasive Lobular Breast Cancer. *Cell* (2015) doi:10.1016/j.cell.2015.09.033.

81. McCart Reed, A. E. *et al.* An epithelial to mesenchymal transition programme does not usually drive the phenotype of invasive lobular carcinomas. *Journal of Pathology* (2016) doi:10.1002/path.4668.

82. Bajrami, I. *et al.* E-Cadherin/ROS1 Inhibitor Synthetic Lethality in Breast Cancer. *Cancer Discov* **8**, 498–515 (2018).

83. da Silva, E. M. *et al.* Abstract P2-23-15: Histologic, immunohistochemical and genomic comparison between classic Invasive lobular carcinomas and lobular-like invasive ductal carcinomas. *Cancer Res* **83**, P2-23–15 (2023).

84. Jiang, Y., Yang, M., Wang, S., Li, X. & Sun, Y. Emerging role of deep learning-based artificial intelligence in tumor pathology. *Cancer Commun* **40**, 154–166 (2020).

85. Couture, H. D. *et al.* Image analysis with deep learning to predict breast cancer grade, ER status, histologic subtype, and intrinsic subtype. *npj Breast Cancer 2018 4:1* **4**, 1–8 (2018).

86. Chan, R. C. K. *et al.* Artificial intelligence in breast cancer histopathology. *Histopathology* **82**, 198–210 (2023).

87. Merritt, C. R. *et al.* Multiplex digital spatial profiling of proteins and RNA in fixed tissue. *Nature Biotechnology 2020 38:5* **38**, 586–599 (2020).

88. da Silva, E. M. *et al.* Mesonephric and mesonephric-like carcinomas of the female genital tract: molecular characterization including cases with mixed histology and matched metastases. *Mod Pathol* **34**, 1570–1587 (2021).

89. da Silva, E. M. *et al.* TERT promoter hotspot mutations and gene amplification in metaplastic breast cancer. *NPJ Breast Cancer* **7**, (2021).

90. Selenica, P. *et al.* APOBEC mutagenesis, kataegis, chromothripsis in EGFR-mutant osimertinib-resistant lung adenocarcinomas. *Ann Oncol* **33**, 1284–1295 (2022).

91. Da Cruz Paula, A. *et al.* Genomic profiling of primary and recurrent adult granulosa cell tumors of the ovary. *Mod Pathol* **33**, 1606–1617 (2020).

92. da Silva, E. M. *et al.* Mesonephric and mesonephric-like carcinomas of the female genital tract: molecular characterization including cases with mixed histology and matched metastases. *Mod Pathol* **34**, 1570–1587 (2021).

93. Zehir, A. *et al.* Mutational landscape of metastatic cancer revealed from prospective clinical sequencing of 10,000 patients. *Nat Med* **23**, 703–713 (2017).

94. Cheng, D. T. *et al.* Memorial Sloan Kettering-Integrated Mutation Profiling of Actionable Cancer Targets (MSK-IMPACT): A Hybridization Capture-Based Next-Generation

Sequencing Clinical Assay for Solid Tumor Molecular Oncology. *The Journal of Molecular Diagnostics* **17**, 251–264 (2015).

95. Li, H. & Durbin, R. Fast and accurate short read alignment with Burrows-Wheeler transform. *Bioinformatics* (2009) doi:10.1093/bioinformatics/btp324.

96. McKenna, A. *et al.* The Genome Analysis Toolkit: a MapReduce framework for analyzing next-generation DNA sequencing data. *Genome Res* **20**, 1297–1303 (2010).

802

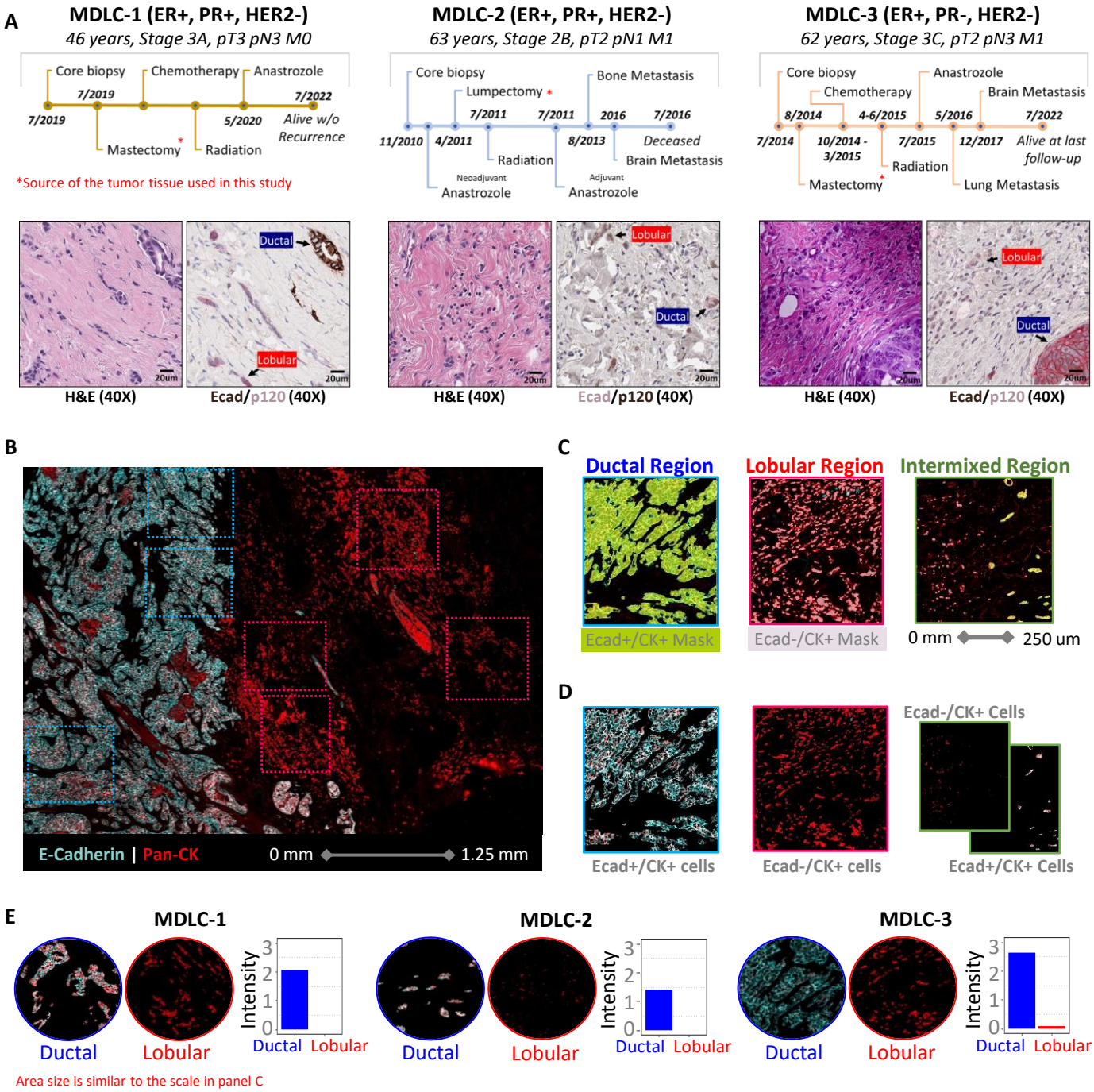

Figure 1. Digital Spatial Profiling of mDLC Ductal and Lobular Tumor Regions.

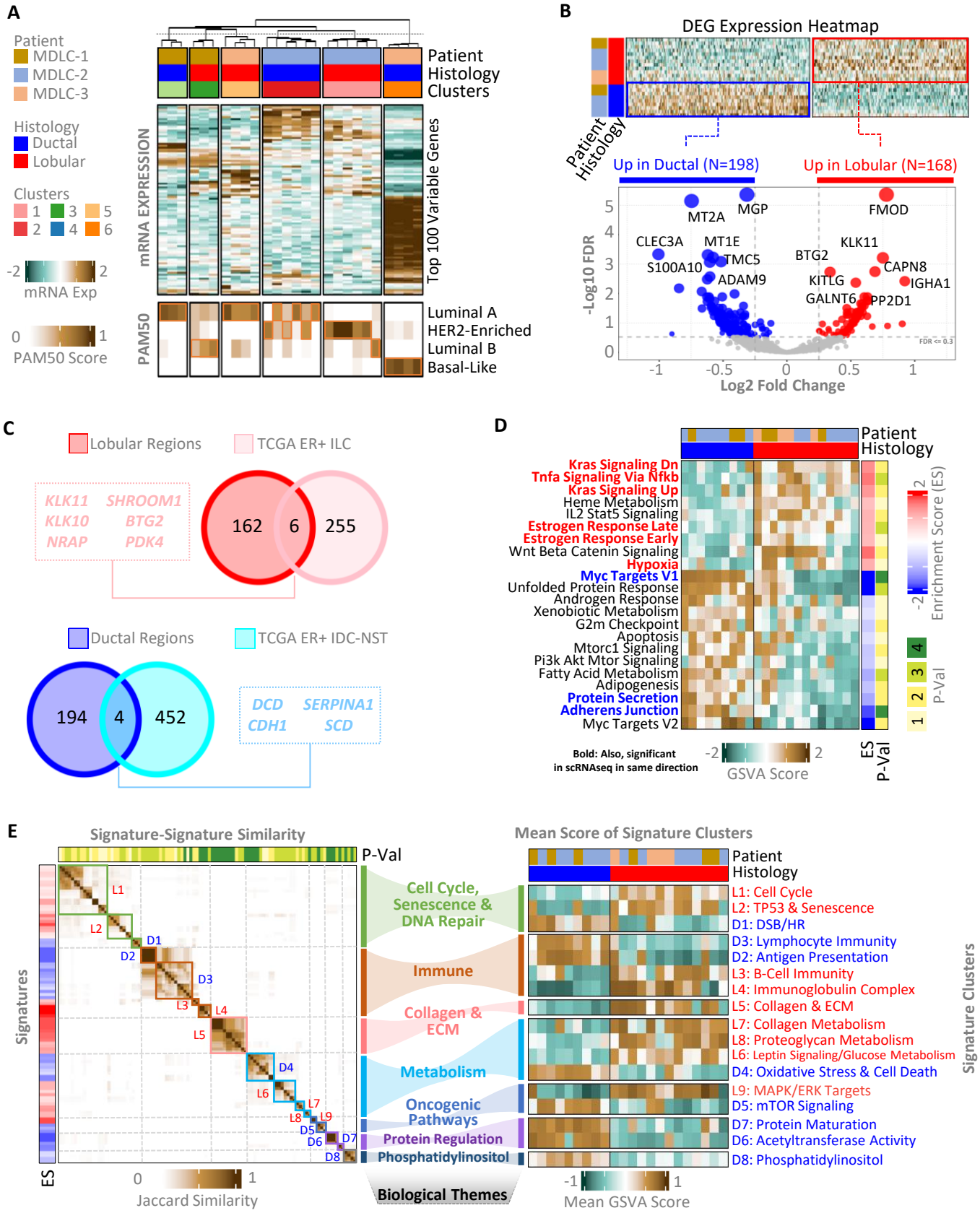

Figure 2. Molecular Subtypes and Distinct Biological Signatures of Ductal and Lobular Tumor Regions.

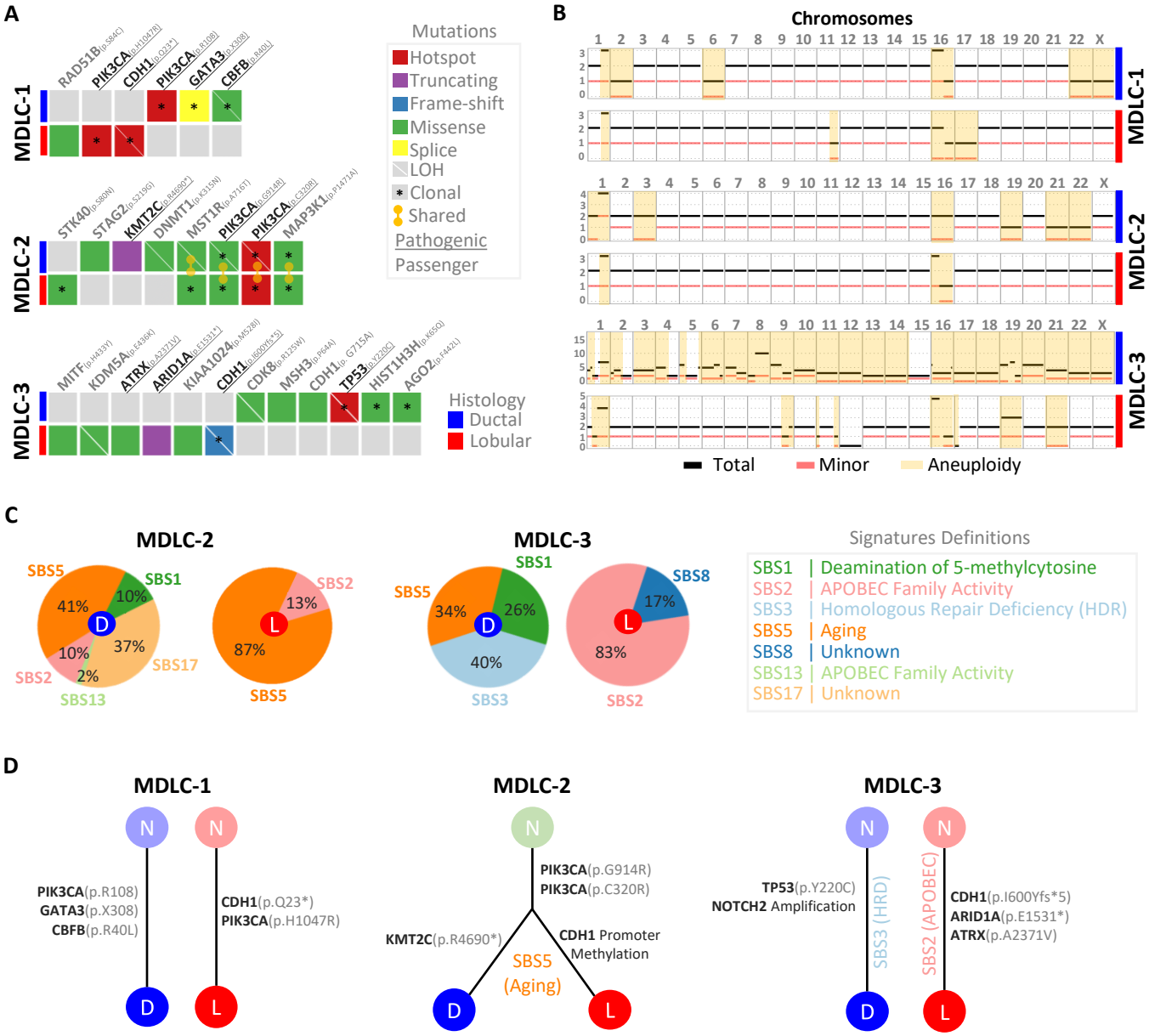

Figure 3. Overview of Genomic Alterations in Ductal and Lobular Tumor Regions.

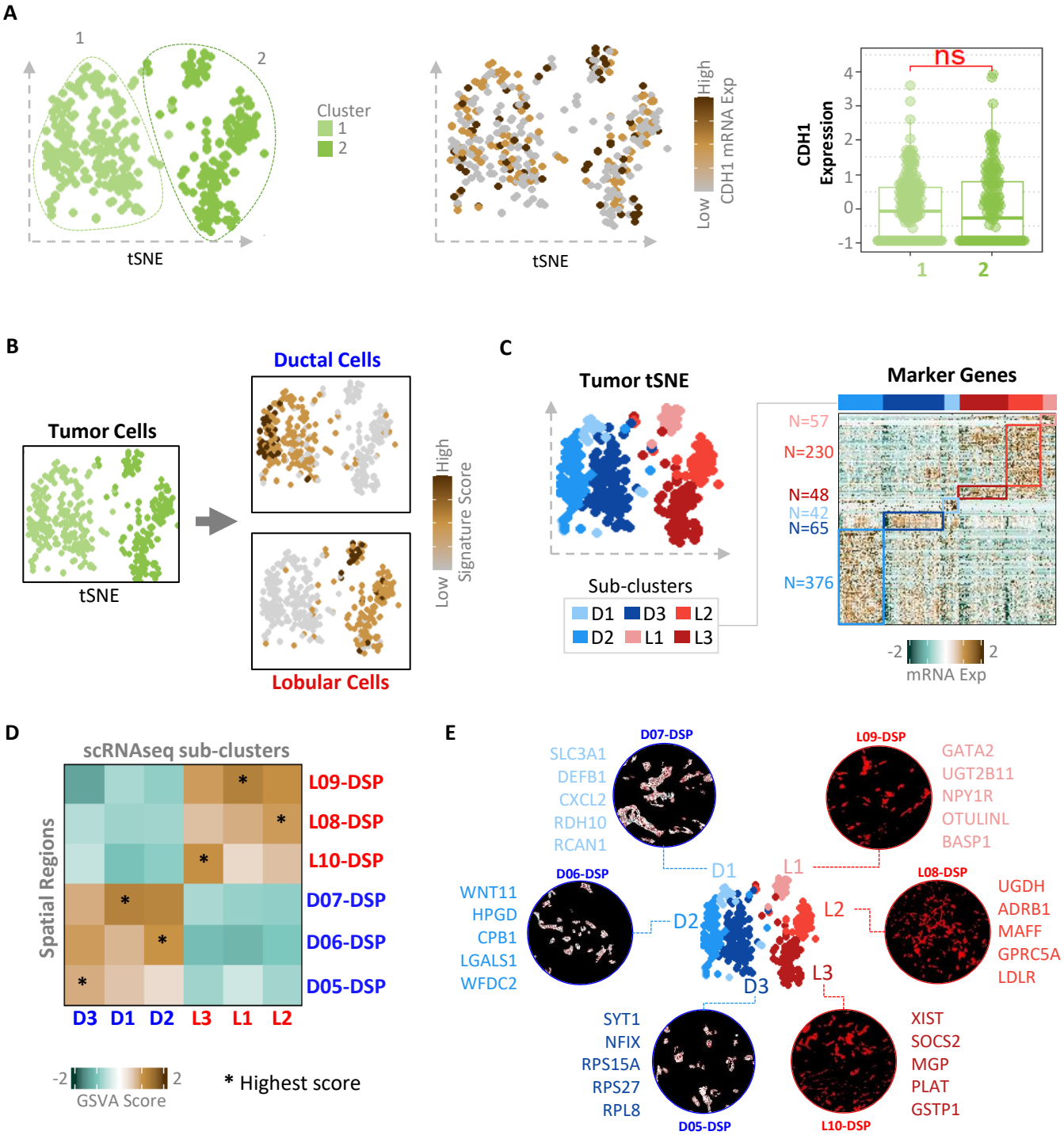

Figure 4: Single Cell Heterogeneity of Ductal and Lobular Tumor Populations.

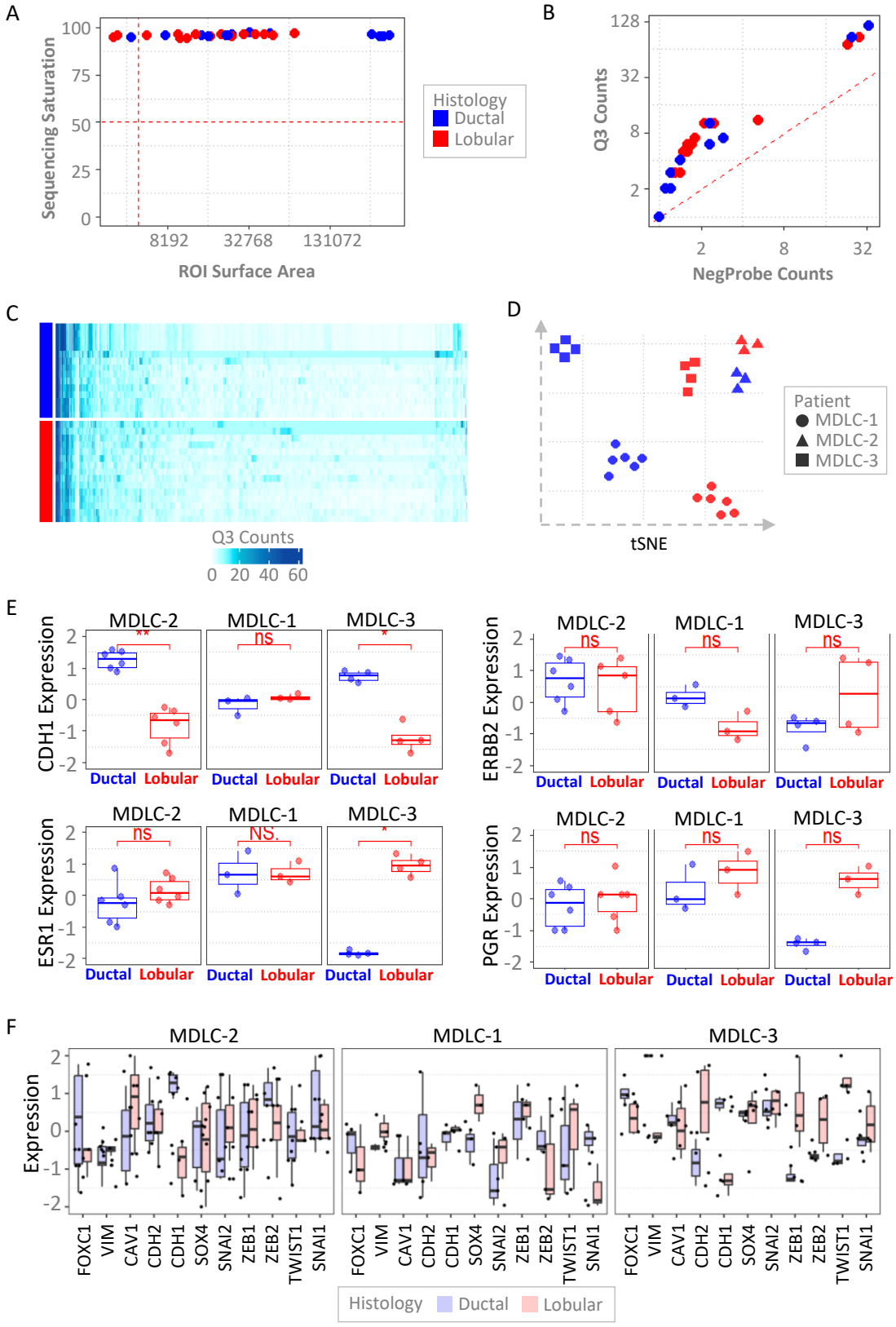

Supplementary Figure S1: Digital Spatial Profiling RNAseq Dataset Quality Control.

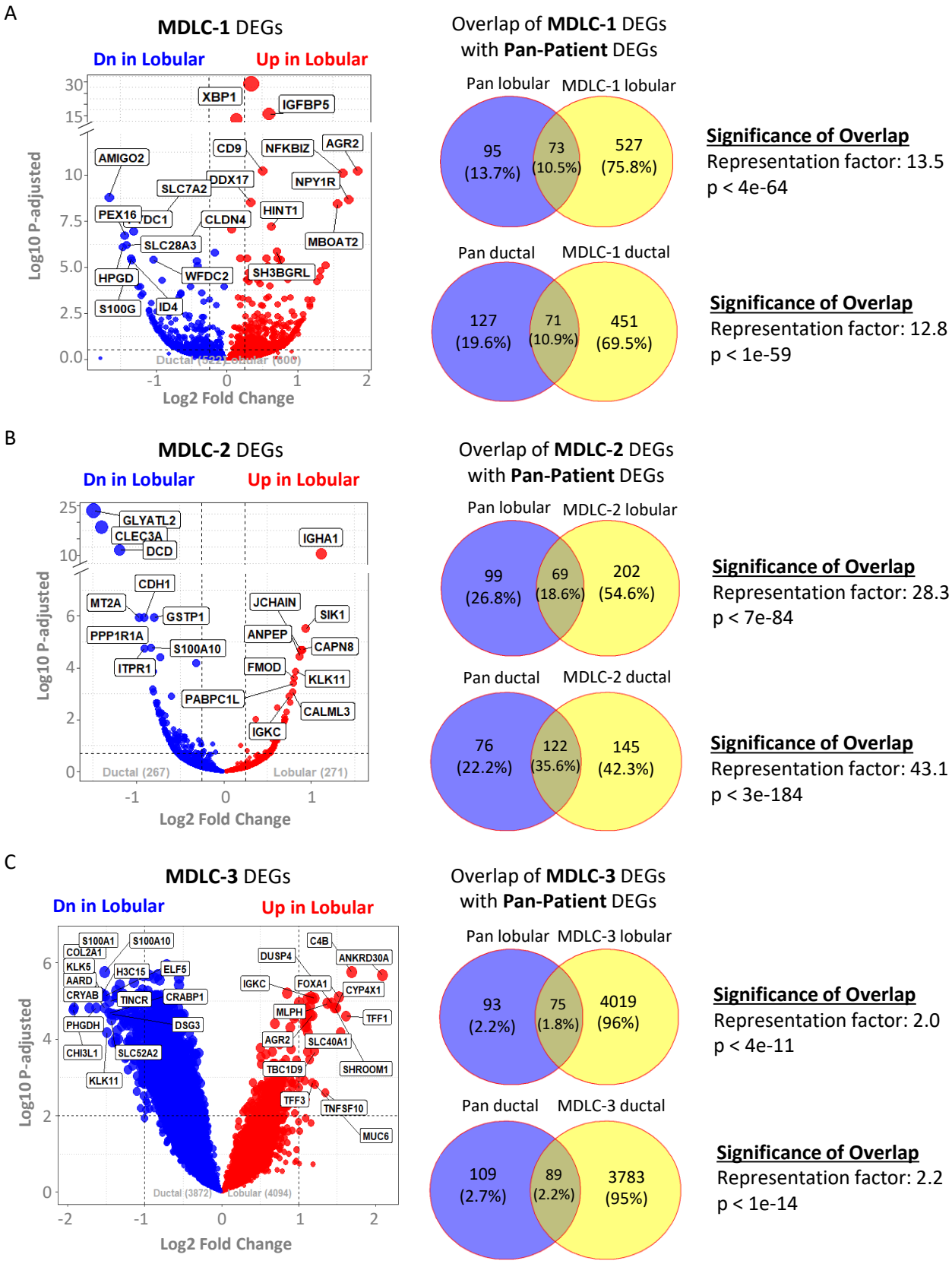

Supplementary Figure S2: Patient Wise Differential Analysis and Comparison with Pan-Patient Differential Analysis.

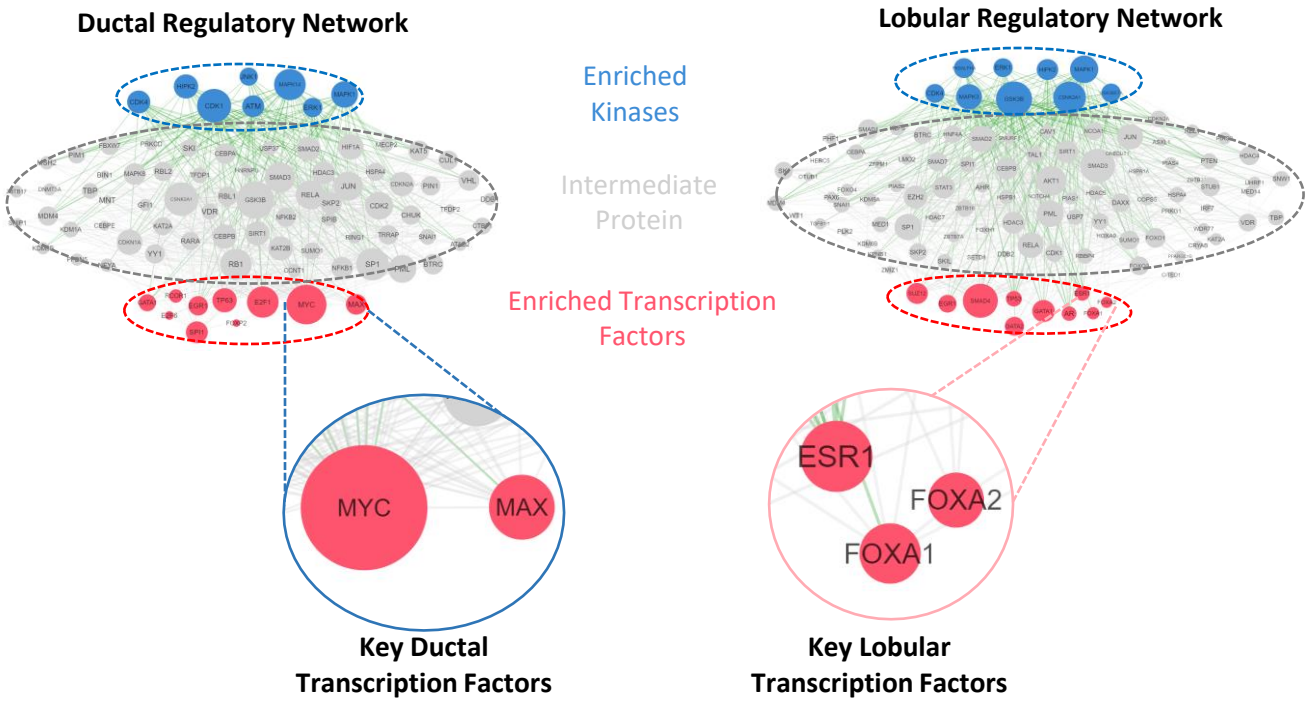

Supplementary Figure S3: Transcription Factor Enrichment Analysis using Pan-Patient Lobular vs Ductal DEGs.

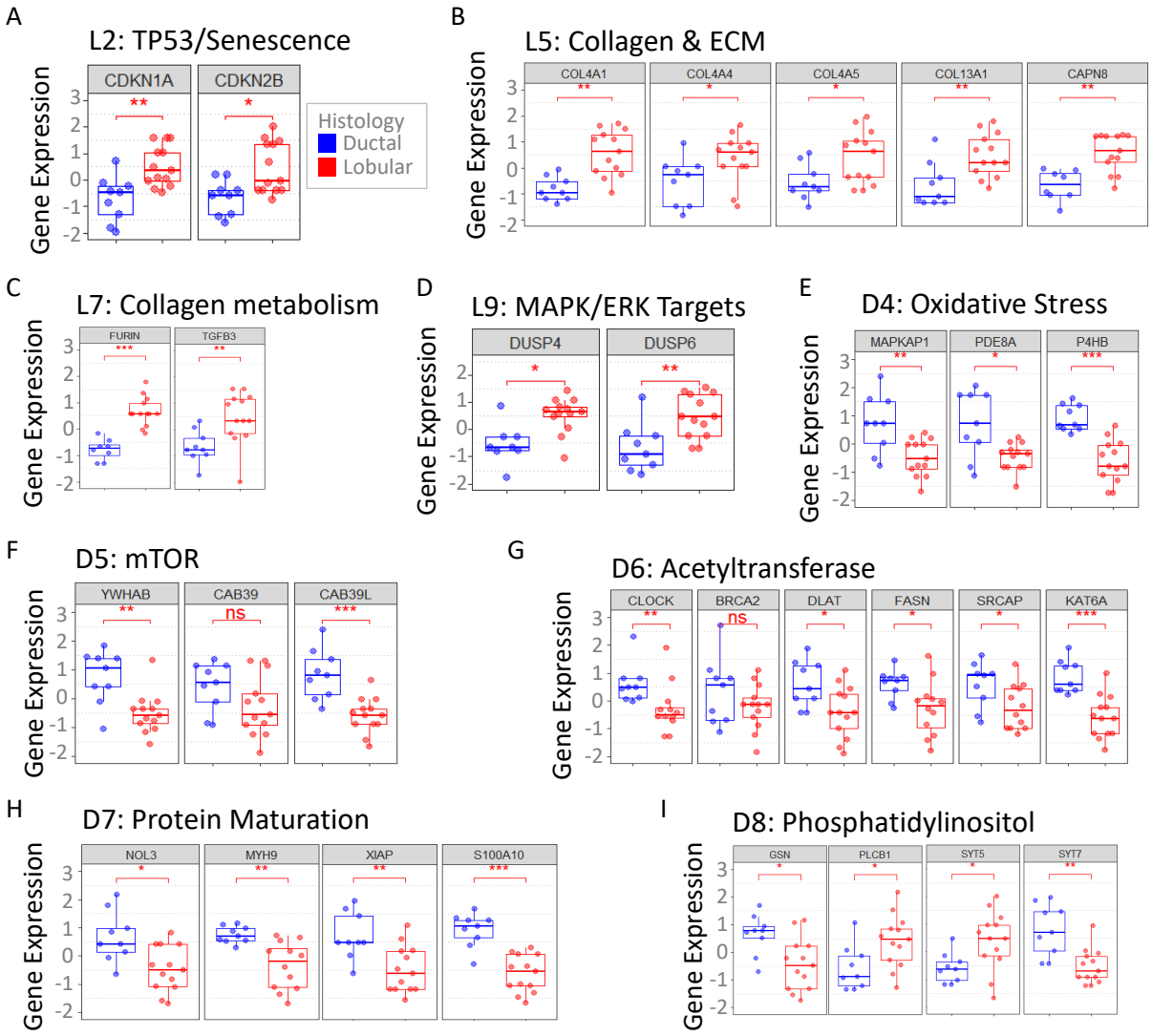

Supplementary Figure S4: Genes Associated with Key Differentially Enriched Biological Signatures.

A

	Sample	Purity	Depth	Ploidy
MDLC-1	Ductal	0.36	428x	2.02
	Lobular	0.45	523x	1.97
MDLC-2	Ductal	0.51	416x	2.04
	Lobular	0.31	339x	2.02
MDLC-3	Ductal	0.62	378x	3.35
	Lobular	0.4	490x	2.01

C

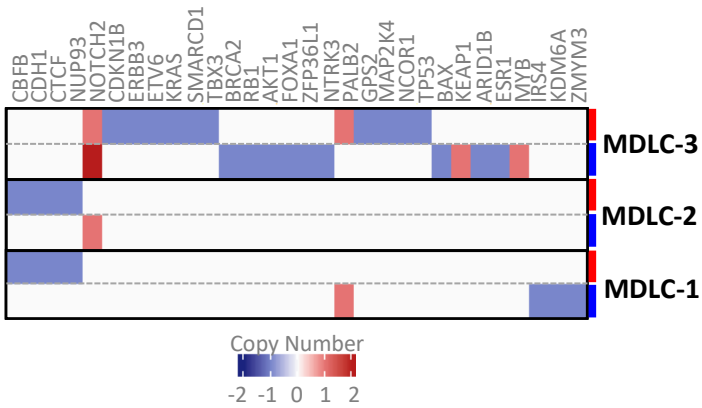

B

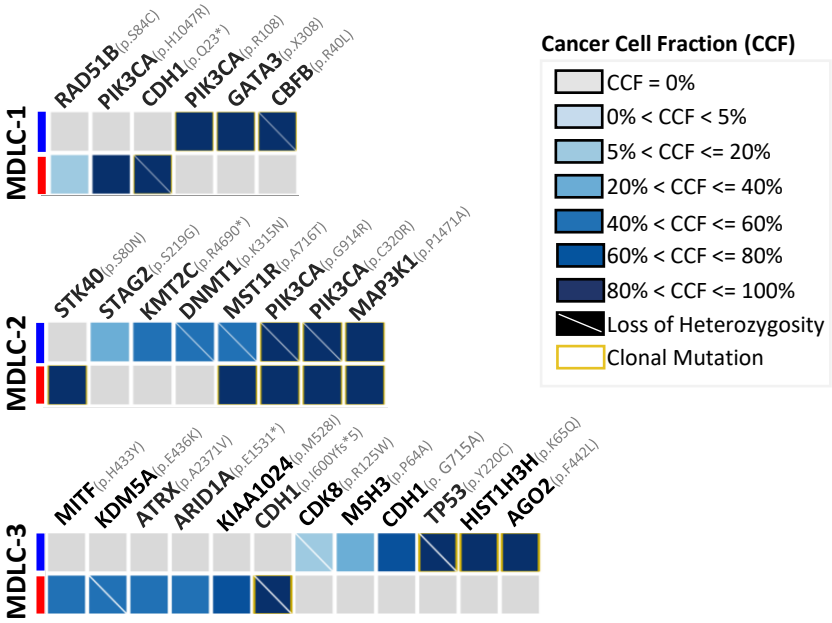

Supplementary Figure S5: MSK Impact Extended Results.

A

Metric	Value
Estimated Number of Cells	4,671
Fraction of Reads in Cells	90.6%
Mean Reads per Cell	91,174
Median Genes per Cell	1,481
Total Genes Detected	24,726
Median UMI Counts per Cell	4,480
Number of reads	425 million
Valid Barcodes	96%
Sequencing Saturation	78.4%

B

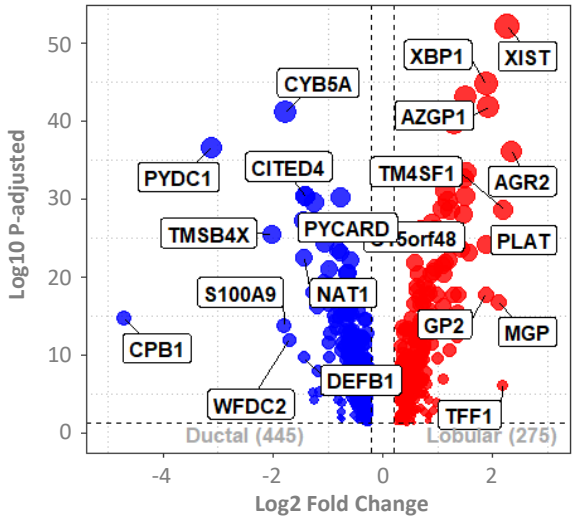

C

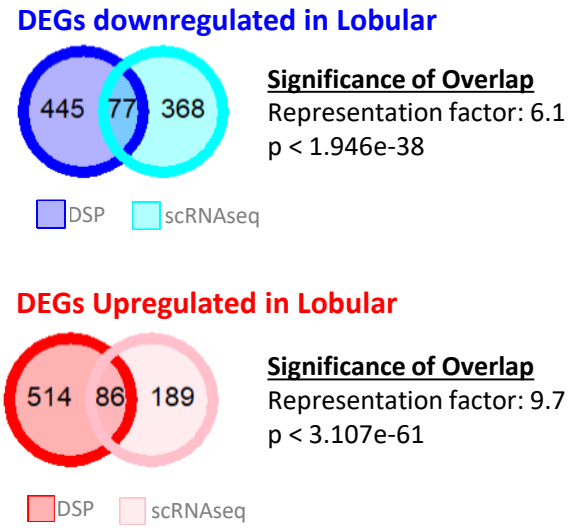

D

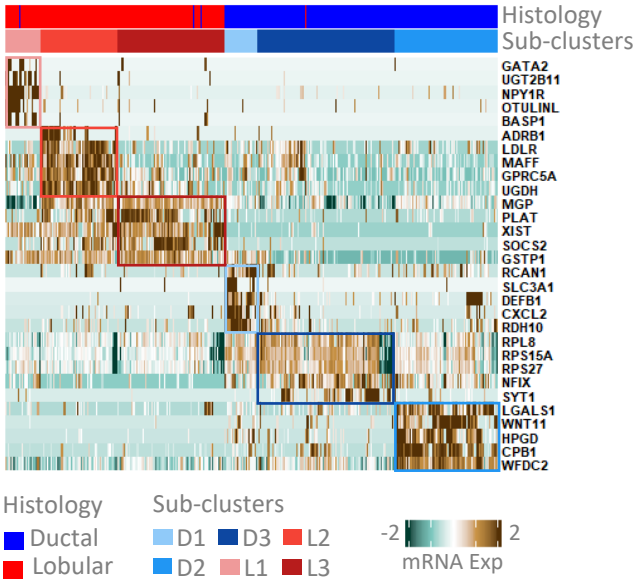

Supplementary Figure S6: MDLC-1 Single-cell RNAseq DEG Analysis and Subcluster Marker Genes.

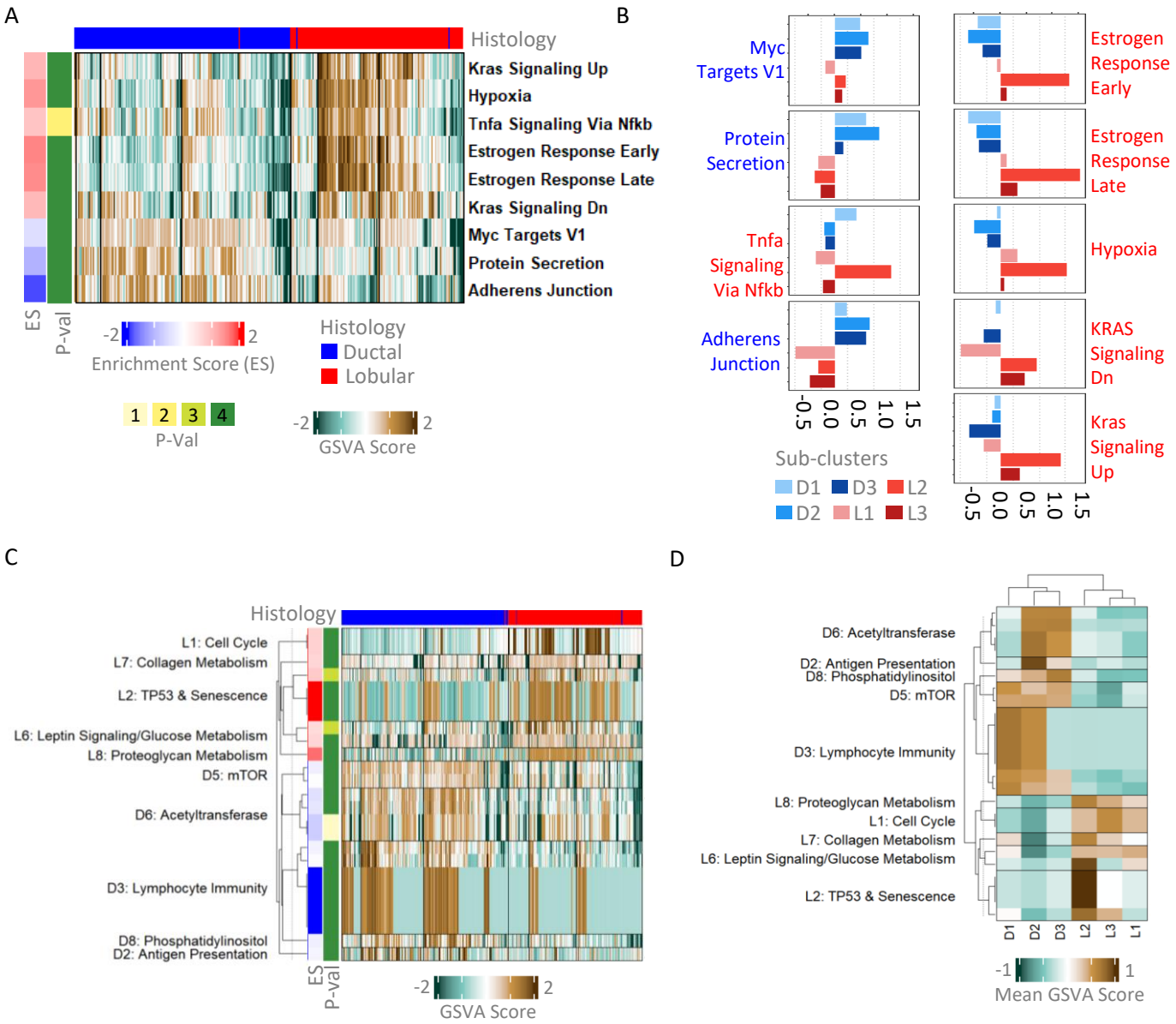

Supplementary Figure S7: MDLC-1 Single-cell RNAseq Pathway Analysis.